Multiphoton imaging of neural structure and activity in *Drosophila* through the intact cuticle

Max Jameson Aragon[1,4,#], Mengran Wang[2,#], Aaron T. Mok[2,#], Jamien Shea[1,#], Haein Kim[1], Nathan Barkdull[3], Chris Xu[2] and Nilay Yapici[1,*]

[1]*Department of Neurobiology and Behavior, Cornell University, 14853, Ithaca, NY, USA*

[2]*School of Applied and Engineering Physics, Cornell University, 14853, Ithaca, NY, USA*

[3]*Department of Physics, University of Florida, 32611, Gainesville, FL, USA*

[4]*Current address: Princeton Neuroscience Institute, Princeton University, 08544, Princeton, NJ, USA*

[#]*These authors contributed equally to this work*

**Corresponding author: Nilay Yapici (ny96@cornell.edu)*

Abstract

We developed a multiphoton imaging method to capture neural structure and activity in behaving flies through the intact cuticles. Our measurements show that the fly head cuticle has surprisingly high transmission at wavelengths > 900 nm, and the difficulty of through-cuticle imaging is due to the air sacs and/or fat tissue underneath the head cuticle. By compressing the air sacs, we performed deep multiphoton imaging of fly brains through the intact cuticle. Our anatomical and functional imaging results show that 2- and 3-photon imaging are comparable in superficial regions such as the mushroom body, but 3-photon imaging is superior in deeper regions such as the central complex and beyond. We further demonstrated 2-photon through-cuticle functional imaging of odor-evoked calcium responses from the mushroom body γ-lobes in behaving flies short-term and long-term (12 consecutive hours). The through-cuticle imaging method developed here extends the time limits of *in vivo* imaging in flies, and opens up new ways to capture neural structure and activity from the intact fly brain.

Introduction

Animal nervous systems across lineages have evolved to solve many of the same problems, such as foraging for food and water, finding mates to reproduce, and avoiding predators to stay alive. They navigate their environment via coordinated movements, and learn and remember the relative values of sensory stimuli around them in order to maximize their fitness and survival. At each instant in time, an animal must evaluate external sensory information and its current behavioral state to decide what to do next (Dickson, 2008; Hunt and Hayden, 2017; Lutcke et al., 2013; McFarland, 1977; Nevin, 1973; Tinbergen, 1969). A major technological challenge to revealing how the brain encodes behavioral states in real-time is that even the simplest neural computation involves interactions across the nervous system at various time scales, while our tools for assessing neural activity are restricted in time and space because of the currently available imaging sensors, methods, and preparations (Lerner et al., 2016). Optical methods remain the most established and fruitful path for revealing population dynamics in neural circuits at long time scales (ranging from minutes to hours) by providing high temporal and spatial resolution measurements (Ji et al., 2016; Luo et al., 2018; Svoboda and Yasuda, 2006).

The fly, *Drosophila melanogaster*, offers an ideal experimental system to investigate neural correlates of behavioral states and decisions because of its compact nervous system and diverse state-dependent behaviors that it executes in response to sensory stimuli (Barron et al., 2015; Dickson, 2008; Yapici et al., 2014). To understand how molecularly defined neural circuits evaluate sensory information in different behavioral states, it is critical to capture the activity of populations of neurons over long time scales as flies are changing their physiological needs (Luo et al., 2018; Simpson and Looger, 2018). These functional imaging experiments require non-invasive imaging preparations, which should allow chronic neural activity imaging for at least 12 hours. Current methods used in fly optical physiology require the fly head cuticle, trachea, and fat body to be removed by microsurgery to provide optical access to the nervous system (Grover et al., 2016; Minocci et al., 2013; Seelig et al., 2010; Sinha et al., 2013; Wang et al., 2003). These preparations are limited in imaging duration because after some time, the brain tissue starts dying due to damaged circulation resulting from the cuticle removal surgery. For example, with current imaging preparations, fly olfactory neurons show reliable Ca^{2+} responses for about four to five hours after surgery (Wang et al., 2003). A non-invasive imaging method and a preparation in which the head cuticle and underlying tissue are left intact, thereby eliminating the need

53 for traumatic head surgery before functional imaging, is essential for advancing fly neuroscience
54 research in the direction of chronic recordings of neural activity during ongoing behaviors. This includes
55 being able to image the same fly brain across multiple days. In mice, multi-day imaging experiments
56 are achieved by implanting a cranial window following removal of part of the skull (Hefendehl et al.,
57 2012; Trachtenberg et al., 2002). Similar imaging preparations have been developed for flies (Grover
58 et al., 2016; Huang et al., 2018; Sinha et al., 2013). However, because imaging window implantation
59 requires a tedious surgery with low success rates and complications that occur afterwards, these
60 methods are not commonly used. A recent development in *in vivo* multiphoton imaging is the use of
61 long wavelength lasers in 3-photon (3P) microscopy which improves the signal-to-background ratio by
62 several orders of magnitude compared to current 2-photon (2P) imaging methods (Horton et al., 2013;
63 Wang et al., 2018a; Wang et al., 2018b). While 3P microscopy with 1700 nm excitation of red
64 fluorophores and adaptive optics has shown promising results in imaging the fly brain through the
65 cuticle (Tao et al., 2017), it is not clear if the technique is widely applicable to common blue and green
66 fluorophores with much shorter excitation wavelengths (e.g. 1320nm).
67
68 Here, we developed a non-invasive method for imaging fly neural structure and activity through
69 the intact head cuticle using both 2P and 3P microscopy. We first measured the ballistic and total optical
70 transmission through the dorsal fly head cuticle and surprisingly found that the head cuticle has high
71 transmission at the wavelengths that are used to excite green fluorophores in 2P and 3P microscopy
72 (~920 nm and ~1320 nm, respectively). We showed that the tissue that interferes with the laser light
73 and limits imaging through the cuticle into the brain is not the head cuticle but the air sacs and the
74 tissue underneath the cuticle. Next, we developed a new imaging method that compresses the air sacs
75 and allows non-invasive, through-cuticle imaging of the fly brain without any surgery. Using this imaging
76 method, we performed deep, high spatial resolution imaging of the fly brain and determined the
77 attenuation length for imaging through the cuticle with 2P (920 nm) and 3P (1320 nm) excitation. Our
78 measurements showed that 2P and 3P excitation performed similarly in shallow regions of the fly brain,
79 but 3P excitation at 1320 nm is superior for deeper brain structures. Furthermore, using 2P and 3P
80 excitation, we imaged food odor evoked neural responses from Kenyon cells comprising the mushroom
81 body γ-lobes using a genetically encoded Ca^{2+} indicator, GCaMP6s (Chen et al., 2013). Kenyon cells
82 are the primary intrinsic neurons in the insect mushroom body. Diverse subtypes of Kenyon cells

83 (n=~2200) extend their axons along the pedunculus and in the dorsal and medial lobes (Crittenden et
84 al., 1998; Ito et al., 1998; Strausfeld et al., 1998). These neurons receive and integrate information from
85 heterogeneous sets of projection neurons which carry olfactory, gustatory, and visual sensory
86 information (Owald and Waddell, 2015; Yagi et al., 2016). In our simultaneous 2P and 3P functional
87 imaging experiments, we found no differences between 2P and 3P excitation, while recording odor
88 evoked responses from the mushroom body γ-lobes through the cuticle. To demonstrate that our non-
89 invasive imaging method can be used for recording neural activity in behaving flies, we used 2P
90 excitation and captured odor evoked neural responses from mushroom body γ-lobes in flies walking on
91 an air suspended spherical treadmill. Finally, we demonstrated long-term functional imaging by reliably
92 capturing odor evoked neural responses from γ-lobes with 2P excitation for 12 consecutive hours. The
93 non-invasive imaging method developed here allows multiphoton imaging of the fly brain without any
94 microsurgery thus, opening up new ways to capture neural structure and activity from the intact fly brain
95 at long time scales and potentially through the entire lifespan of flies.
96
97 **Results**
98 **Fly head cuticle transmits long wavelength light with high efficiency**
99 To develop a non-invasive imaging method using multiphoton microscopy, we first measured light
100 transmission at different wavelengths through the fly head cuticle. Previous experiments showed that,
101 within the wavelength range of 350 nm to 1000 nm, the relative transmission of the dorsal head cuticle
102 of *Drosophila melanogaster* increases with increasing wavelengths (Lin et al., 2015), however, the
103 absolute transmission, which is critical for assessing the practicality of through-cuticle imaging, was not
104 reported. In our experiments, we quantified both the total and ballistic transmission of infrared (IR) lights
105 through the cuticle. Dissected head cuticle samples were mounted between two glass coverslips and
106 placed in the beam path between the laser source and the photodetector (Figure 1A). The total and
107 ballistic transmission through the cuticle samples were measured using a custom-built system (Figure
108 1B). For ballistic transmission, light from a single-mode fiber was magnified and focused on the cuticle
109 with a ~25μm spot size. Figure 1C illustrates the light path of ballistic transmission experiments. The
110 sample stage was translated to obtain measurements at different locations on the head cuticle. Ballistic
111 transmission through the cuticle was measured at seven different wavelengths (852 nm, 911 nm, 980

112 nm, 1056 nm, 1300 nm, 1552 nm, 1624 nm) that match the excitation wavelengths for typical 2P and
113 3P imaging. We found that for all the IR wavelengths tested, the ballistic transmission through the
114 cuticle was high, reaching >90% at 1300 nm (Figure 1D). Since fluorescence signal within the focal
115 volume in 2P- and 3P-microscopy is mostly generated by the ballistic photons (Dong et al., 2003;
116 Horton et al., 2013), our results showed that ballistic photon attenuation by the fly cuticle does not limit
117 multiphoton imaging through the intact cuticle.
118
119 To assess the absorption properties, we measured the total transmission through the head
120 cuticle. For these measurements, laser light from a single mode fiber was magnified and focused on
121 the cuticle sample with a ~50μm spot size. An integrating sphere was placed immediately after the
122 cuticle to measure the total transmission. Figure 1F illustrates the light path of total transmission
123 experiments. Total transmission through the cuticle was measured at nine different wavelengths (514
124 nm, 630 nm, 852 nm, 911 nm, 980 nm, 1056 nm, 1300 nm, 1552 nm, 1624 nm). The shorter
125 wavelengths of 514 nm and 630 nm were chosen to match the typical fluorescence emission
126 wavelengths of green and red fluorophores. Similar to the ballistic transmission experiments, we found
127 that the total transmission generally increases with wavelength (Figure 1G), and the total transmission
128 for both the green and red wavelengths was sufficiently high (>60%) for practical epi-fluorescence
129 imaging using 2P or 3P excitation. We also scanned the cuticle with a motorized stage in the setup at
130 selected wavelengths (Figure 1E, H), and these spatially-resolved transmission map confirmed that
131 there are only a few localized regions at the periphery of the cuticle with low transmission. Our results
132 demonstrated that absorption and scattering of long wavelength light by the *Drosophila* head cuticle is
133 small, and non-invasive *in vivo* imaging of green (e.g., GFP and GCaMP) and red fluorophores (e.g.,
134 RFP, RCaMP) through the cuticle is possible in adult flies using 2P or 3P excitation.

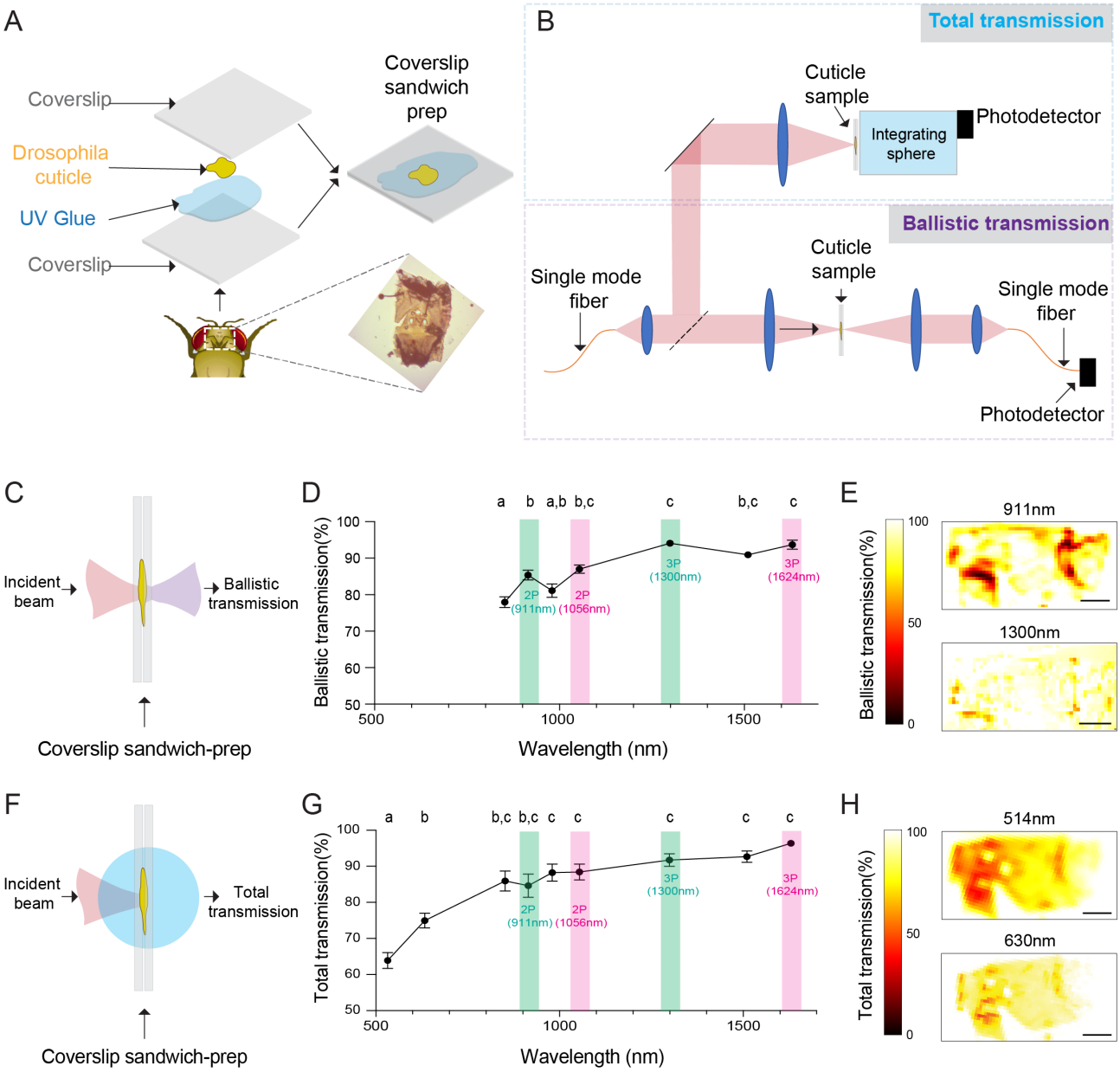

Figure 1: Ballistic and total optical transmission of the fly head cuticle. (**A**) Schematic of the cuticle preparation. (**B**) Schematic of the cuticle optical transmission measurement setup. (**C**) Schematic of the ballistic optical transmission through the cuticle. (**D**) Results of the ballistic optical transmission experiments at various wavelengths (n = 56 measurements at each wavelength, 5 different samples). (**E**) Spatially-resolved maps at 911 nm and 1300 nm with the percent ballistic transmission color coded. Lighter colors indicate higher transmission and darker colors indicate lower transmission. (**F**) Schematic of the total optical transmission through the cuticle. (**G**) Results of the total optical transmission experiments at various wavelengths (n = 20 measurements at each wavelength, 4 different samples). (**H**) Spatially-resolved maps at 514 nm and 630 nm with the percent total transmission color coded. Lighter colors indicate higher transmission and darker colors indicate lower transmission. One-way ANOVA with post-hoc Tukey's test. Significantly different groups are labeled with different letters in D and G. Scale bars =100μm.

147 **Through-cuticle structural multiphoton imaging of the fly brain**

148 Based on our cuticle transmission results, we developed a non-invasive imaging method where
149 we used head compression to minimize the volume of the air sacs and the tissue between the head
150 cuticle and the brain (Figure 2A, Video 1). We imaged the fly brain in vivo through the cuticle with no
151 head compression, semi-compression, or full-compression (Figure 2B-D). We expressed membrane-
152 targeted GFP selectively in mushroom body Kenyon cells and imaged the fly brain through the cuticle
153 using 2P and 3P excitation at 920 nm and 1320 nm, respectively (Figure 2E-G). Mushroom body
154 Kenyon cells are bilaterally symmetric groups of neurons that are subdivided according to their axonal
155 trajectories. The cell bodies of these neurons are located around the calyx of the mushroom bodies.
156 Kenyon cell dendrites arborize in the calyx, while their axons fasciculate into anatomically distinct
157 structures called lobes, with the dorsal lobes forming α and α′ branches, and the medial lobes
158 containing β, β′, and γ branches (Crittenden et al., 1998; Ito et al., 1998; Zheng et al., 2018). We used
159 transgenic flies that specifically expressed GFP in Kenyon cells forming α, β and γ lobes (Krashes et
160 al., 2007). In non-compressed flies, the mushroom body lobes were barely visible in both 2P and 3P
161 imaged flies. Compressing the head against the cover-glass with forceps during the curing process
162 drastically improved image quality (Figure 2E-G). Based on our observations of the leg movements,
163 flies behaved similarly in semi-compressed and non-compressed preps but not in full compression, and
164 mushroom body lobes were only visible in semi-compressed preps. Thus, unless explicitly stated (e.g.,
165 for the purpose of comparisons), we used semi-compressed preps in the structural and functional
166 imaging experiments reported in this paper.

167

168 We also investigated why head compression improves image quality in intact flies. We
169 hypothesized, head compression reduces the volume of air sacs and surrounding tissue between the
170 cuticle and the brain, allowing better transmission of the long wavelength laser light through these
171 structures. To test our hypothesis, we surgically removed air sacs from one side of the fly head and
172 imaged the brain using 2P and 3P excitation without any head compression. As predicted, we were
173 able to image the mushroom body lobes on the side where air sacs were removed but not on the side
174 where intact air sacs were present (Figure 2- figure supplement 1A-C, Video 2). Our results
175 demonstrated that the tissue that interferes with 2P and 3P laser light is not the cuticle itself but the air
176 sacs and tissues that are between the head cuticle and the brain.

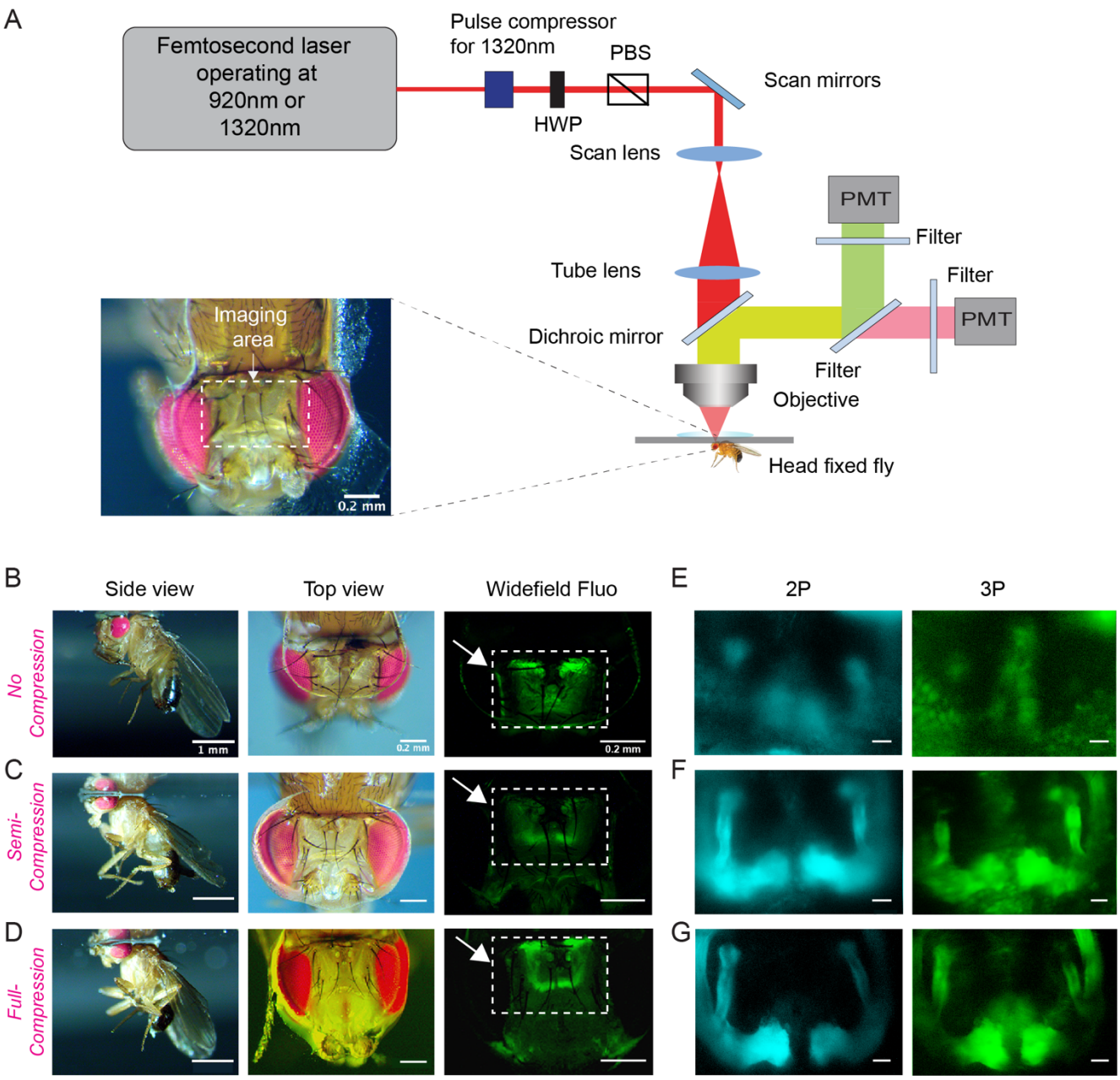

Figure 2. **Through-cuticle imaging of the fly brain with 2P and 3P excitation. (A),** Schematic of the multiphoton microscope setup. Fly head is fixed to a cover slip and placed under the objective (HWP: half-wave plate, PBS: polarization beam splitter, PMT: photomultiplier tube). The imaging window on the fly head is shown in the picture (lower left). Scale bar = 200μm **(B-D)**, The head-uncompressed and head-compressed imaging preparations. The first column shows the side image of the fly that is head fixed to the cover glass (scale bar =1mm). The second and third columns show the fly head visualized under a brightfield (top view) and fluorescent dissecting microscopes (widefield-fluo), respectively. Arrows and the rectangle area in widefield-fluo column indicate the imaging window (scale bar=200μm). (**E-G),** Cross section imaging of the mushroom body (MB) Kenyon cells expressing CD8-GFP through the head cuticle at 920 nm (2P) and 1320 nm (3P) excitation. The Z projections of 2P (cyan, left) and 3P (green, right) imaging stacks. For each imaging preparation, the same fly head is imaged with 3P excitation and 2P excitation (scale bar=20μm).

189 **Comparison of 2P and 3P excitation for deep brain imaging through the fly head cuticle**

190 Our non-invasive imaging experiments showed that through–cuticle imaging is possible with both 2P
191 and 3P excitation. In general, 3P excitation requires higher pulse energy at the focal plane compared
192 to 2P excitation because of the higher-order nonlinearity. On the other hand, longer wavelength (1320
193 nm) used for 3P excitation can experience less attenuation while travelling in the brain tissue leading
194 to increase tissue penetrance and imaging depth (Wang et al., 2018a). To compare the performance
195 of 2P and 3P excitation for through-cuticle imaging, we imaged the entire brain in a fly expressing
196 membrane-targeted GFP pan neuronally. Figure 3A shows the images from the same fly brain at
197 different depths with 2P (920 nm) and 3P (1320 nm) excitation. At the superficial brain areas such as
198 the mushroom bodies, 2P and 3P excitation performed similarly. As we imaged deeper in the brain, 3P
199 excitation generated images with higher contrast compared to 2P excitation and was capable of
200 imaging brain regions below the esophagus (~ 225 μm below the surface of head cuticle) while
201 maintaining high spatial resolution. We further quantified the effective attenuation length (EAL) for 2P
202 and 3P excitation, and we found EAL_{920nm}= 41.7 μm, EAL_{1320nm}= 59.3 μm within depth 1-100μm, and
203 EAL_{1320nm}= 91.7 μm within depth 100-180μm (Figure 3B). The third harmonic generation (THG) signal
204 from the head cuticle and the brain trachea was also measured as a function of depth. THG signal can
205 be used to measure the EAL (EAL_{THG}) (Yildirim et al., 2019). The EAL_{THG} within the cuticle was much
206 larger than the EAL_{THG} inside the brain, once again demonstrating the high ballistic transmission of the
207 1320 nm laser light through the head cuticle (Figure 3C). The full width at half maximum (FWHM) of
208 the lateral brightness distribution at 200μm below the surface of the head cuticle was ~1.4μm for
209 tracheal branches captured by the THG signal (Figure 3D). Similarity in the attenuation lengths
210 measured with THG and 3P fluorescence signal indicates that the labelling of membrane-targeted GFP
211 is uniform across the brain, validating the use of the fluorescence signal when quantifying the EALs.

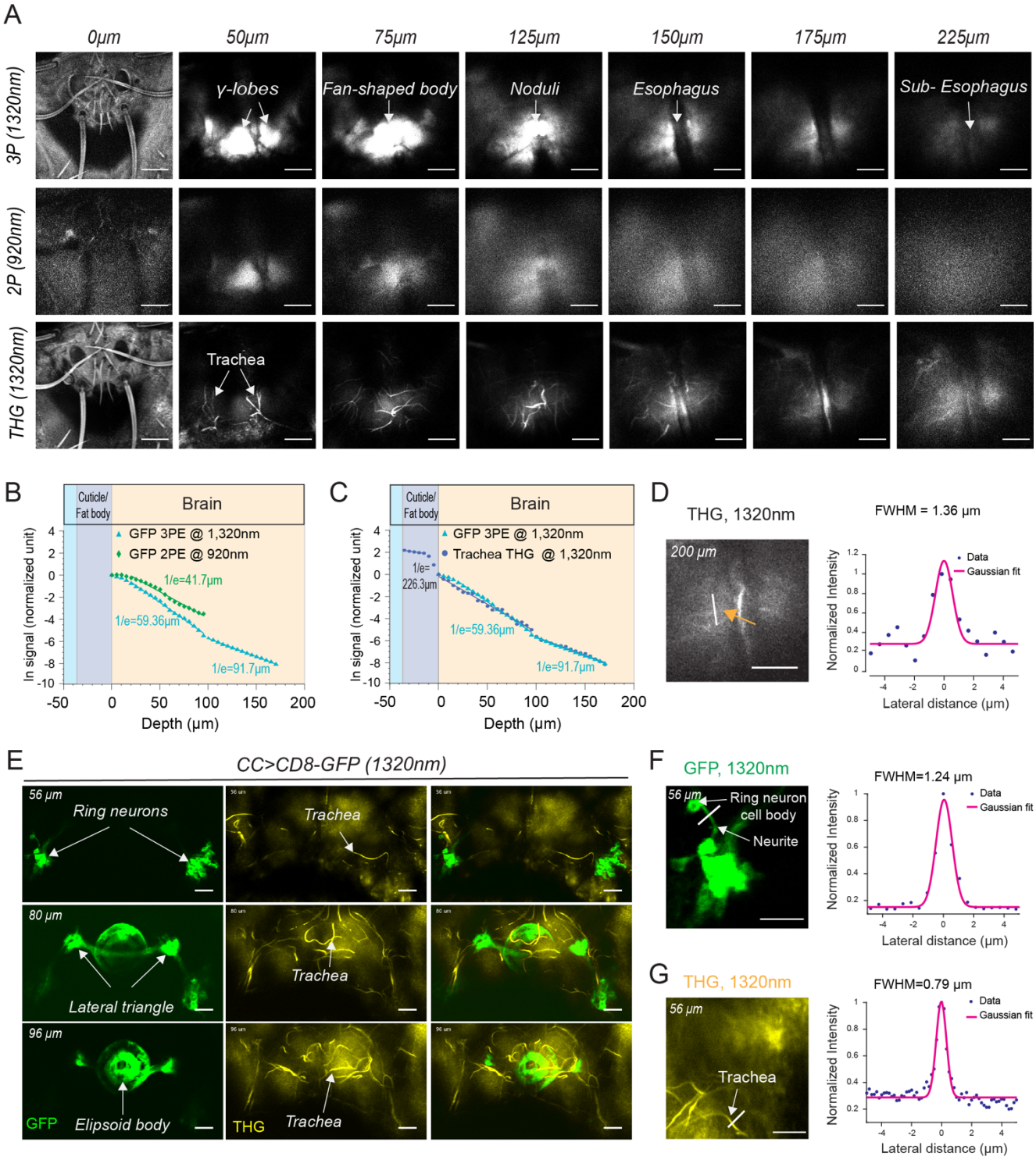

Figure 3. 2P and 3P structural imaging of the fly brain. (A) Cross section images of the fly brain through the cuticle with 3P (top) and 2P (bottom) excitation at different depth. The THG images are included at the bottom. 3P excitation power is < 11mW and the repetition rate is 333 kHz. 2P excitation power is < 15mW and the repetition rate is 80 MHz. Scale bars = 50μm. (**B**) GFP signal as a function of depth for 920 nm 2P excitation and 1320 nm 3P excitation. (**C**) Comparison of the GFP signal and THG signal as a function of depth at 1320 nm. (**D**) Lateral resolution measurement in the THG image captured at 200μm depth**.** Lateral intensity profile measured along the white line (indicated by the orange arrow) is fitted by a Gaussian profile for the lateral resolution estimation (scale bar=50μm). **(E)** Cross section images of the central complex (CC) ring neurons through the cuticle with 1320 nm 3P excitation (green). Third harmonic generation (THG) imaging visualizes the tracheal arbors (yellow). Arrows indicate different CC compartments that are identified (scale bars= 30μm). (**F-G**) Lateral resolution measurements in 3P images captured at 56μm depth. **(F)** The GFP fluorescence profile of CC ring neurons (green) and **(G)** the THG profile of surrounding trachea (yellow). Lateral intensity profiles measured along the white lines are fitted by Gaussian profiles for the lateral resolution estimation (scale bars=20μm).

212 To further compare the performance of 2P and 3P excitation for through-cuticle imaging in
213 deeper brain neuropils, we imaged central complex ellipsoid body neurons. The insect central complex
214 is a brain neuropil which processes sensory information and guides a diverse set of behavioral
215 responses which include navigation, walking initiation, and turning direction (Pfeiffer and Homberg,
216 2014; Seelig and Jayaraman, 2015; Wolff et al., 2015). It is composed of anatomically distinct
217 compartments: the protocerebral bridge, ellipsoid body, fan-shaped body, and the noduli (Wolff et al.,
218 2015). The ellipsoid body consists of a group of neurons, the ring neurons, that extend their axons to
219 the midline and form a ring-like structure that is composed of different layers (Pfeiffer and Homberg,
220 2014; Wolff et al., 2015; Xie et al., 2017). Using an ellipsoid body-specific promoter, we expressed
221 membrane-targeted GFP in the fly brain and imaged the ring neurons with 2P and 3P excitation.
222 Compared with 3P excitation (Figure 3E), the resolution and contrast of images taken by 2P excitation
223 is reduced when imaging through the cuticle at this depth (Figure 3-figure supplement 1A-B). Ring
224 neuron cell bodies, as well as the lateral triangle and the ellipsoid body layers, are clearly visible when
225 3P excitation was used (Figure 3E, Video 3). Using ring neuron arbors and tracheal branches, we
226 estimated the lateral resolution of the 3P images. The FWHM of the lateral brightness distribution
227 measured by a ring neuron's neurite cross section was ~1.2μm for the fluorescent signal (Figure 3F)
228 and ~0.8μm for tracheal branches captured by the THG signal (Figure 3G). Our results demonstrate
229 that although both 2P and 3P excitation can be used to image through the cuticle for the superficial
230 layers of the fly brain such as the mushroom body, 3P excitation outperforms 2P excitation in deeper
231 brain regions such as the central complex. This conclusion is similar to that observed in the mouse
232 brains (Mok et al., 2019; Wang et al., 2018a; Wang et al., 2020).

233 **Simultaneous 2P and 3P imaging of odor-evoked responses from Mushroom body γ-lobes**

234 We next compared 2P and 3P excitation to capture neural activity in the fly brain through the intact
235 head cuticle. In these experiments, a custom odor delivery system was used where flies were head
236 fixed and standing on a polymer ball under the microscope (Figure 4A-B). We expressed GCaMP6s
237 selectively in Mushroom body Kenyon cells and stimulated the fly olfactory sensory organ, the antenna,
238 with the food odor apple cider vinegar (Figure 4C-F). Using a multiphoton microscope, odor evoked
239 Ca^{2+} responses of mushroom body γ-lobes were simultaneously captured with 2P (920 nm) and 3P
240 (1320 nm) excitation using the temporal multiplexing technique (Ouzounov et al., 2017).

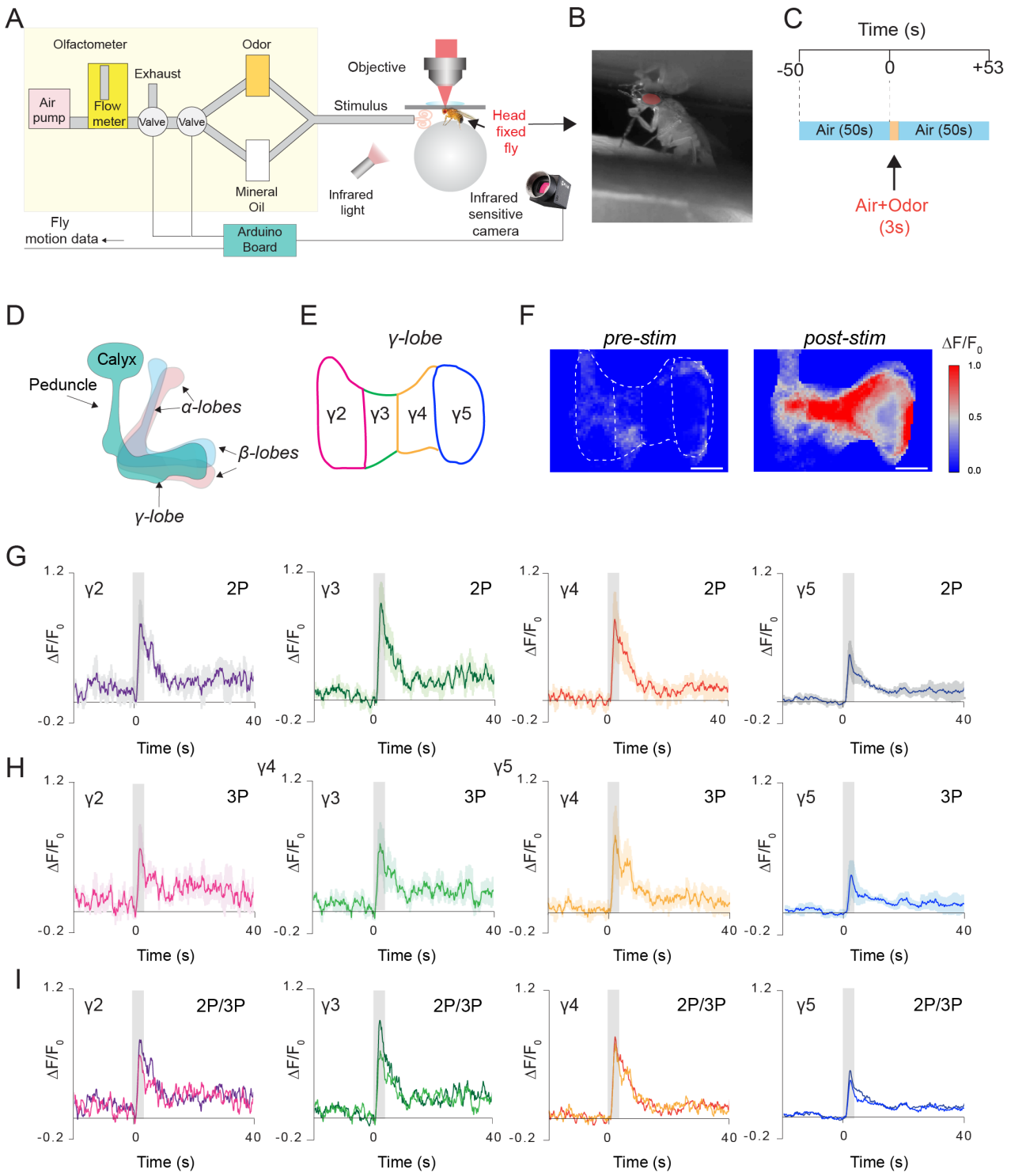

Figure 4. Simultaneous 2P and 3P functional imaging of short-term odor-evoked responses of the mushroom body Kenyon cells. (A) Schematic of the custom made olfactometer and the through-cuticle functional imaging setup. (**B**) Picture of the head-fixed fly on the ball under the multiphoton microscope. (**C**) Stimulus timeline. The same stimulus scheme was repeated 5 times using the same odor. (**D**) Schematic of the mushroom body anatomy indicating the locations of α, β, and γ lobes. **(E)** γ-lobes have discrete anatomical compartments (shown as γ2–γ5). **(F)** GCaMP6s is expressed in the mushroom body Kenyon cells. Normalized ($\Delta F/F_0$) GCaMP6s signal is shown before (left) and after (right) odor stimulus (scale bar= 20 μm). **(G)** Odor-evoked responses of Kenyon cells captured by 2P excitation at 920 nm and **(H)** 3P excitation at 1320 nm. **(I)** Comparison of the average responses captured by simultaneous 2P and 3P imaging over time (n=3 flies, 4-5 trials per fly, data are presented as mean ± SEM in (**G**) and (**H**), grey bar indicates when stimulus is present). Average laser powers are 5 mW at 920 nm and 4 mW at 1320 nm.

241 A brief 3s odor stimulus triggered a robust fluorescence increase in Kenyon cell axons comprising the
242 mushroom body γ-lobes (Figure 4F). Kenyon cell axons are innervated by distinct subsets of
243 dopaminergic neurons, which carry contextual information to the mushroom body depending on the
244 fly's previous experiences. Based on dopaminergic innervation, γ-lobes can be subdivided into five
245 anatomical compartments (Cohn et al., 2015) (Figure 4D-E). To determine whether the localized
246 dopaminergic input along the Kenyon cell axons impacts the olfactory responses in the γ-lobes, we
247 visualized the normalized fluorescence signal in each compartment of the γ-lobes. No significant
248 differences were observed in neural responses to food odor stimulation across different compartments
249 of the mushroom body or between 2P and 3P excitation of GCaMP6s (Figure 4G-I). Our data
250 demonstrated that it is not necessary to use 3P imaging at 1320 nm for through-cuticle imaging of the
251 mushroom body. The sample preparation technique developed here enabled conventional 2P imaging
252 at 920 nm to capture odor evoked Ca^{2+} responses in the mushroom body through the intact cuticle with
253 temporal resolution comparable to 2P microscopy with the open cuticle preparations (Cohn et al., 2015;
254 Wang et al., 2003).
255
256 **Average power limit of 3P imaging in the fly brain**
257 2P imaging has been widely used in fly neuroscience research. The recommended power level
258 for 2P imaging of fly neural activity is below 15mW (Seelig et al., 2010). However, it is not clear, how
259 3P excitation impacts the fly brain. It has been shown 3P excitation can induce heating in the mouse
260 brain at high laser powers (Wang et al., 2018a; Wang et al., 2018b; Wang et al., 2020). Therefore, we
261 measured how heat generated by 3P excitation impacts the fly brain using HSP70 protein as a marker
262 for cellular stress response (Lindquist, 1980; Podgorski and Ranganathan, 2016). We first tested
263 whether HSP70 protein levels reflect heat induced stress response in the fly brain cells by placing flies
264 in a 30°C incubator for 10 minutes and staining for HSP70 protein right after the incubation. Flies that
265 were kept at room temperature had low levels of the HSP70 protein in a very small number of cells in
266 the brain (Figure 4-figure supplement 1A). In contrast, placing flies in a 30°C incubator for 10 minutes
267 caused a significant increase in the number of HSP70 positive neurons and an elevation of HSP70
268 protein levels across the fly brain (Figure 4-figure supplement 1B). Next, we tested whether 3P
269 excitation can elevate HSP70 protein levels similar to heat induced stress in fly neurons. Head-fixed

flies in a semi-compressed imaging prep were imaged for 10 minutes using 3P excitation at 1320 nm. Our results showed that there was no measurable heat-stress response detected by the HSP70 protein levels at the power levels < 20mW. (Figure 4-figure supplement 1C). However, increasing laser power to > 25mW caused structural abnormalities and a significant increase in HSP70 protein levels in the fly brain (Figure 4-figure supplement 2D). These results suggested that 3P non-invasive imaging of the fly brain is safe at power levels below 20mW, which is approximately 2x higher than the power we used for the deepest 3P imaging (Fig. 3A).

2P through-cuticle imaging captures odor evoked responses in behaving flies

To investigate how head compression impacts fly behavior and neural activity, we investigated how flies that are head-compressed but allowed to walk on a spherical treadmill respond to an odor stimulation. Using our custom behavior/imaging setup (Figure 5A), we stimulated the fly antennae that are fully exposed with food odor (apple cider vinegar), while recording neural activity from the mushroom body γ-lobes using 2P excitation (920 nm) through the head cuticle and capturing fly's behavioral responses using a camera that is synchronized with the 2P microscope. In these experiments, a head fixed fly was continuously exposed to a low-speed air flow before and after the 3s odor stimulus with the same air flow speed, and the behavioral responses of flies were captured by tracking the spherical treadmill motion using the FicTrac software during each trial (Video 4). Because internal states impact behavioral responses to food odors (Lin et al., 2019; Sayin et al., 2019), we used flies that are 24-hour food deprived. Previous studies have demonstrated that during food odor exposure, hungry flies increase their walking speed, orient and walk towards the odor stimulus. After odor stimulation however, flies increase their turning rate which resembles local search behavior. The odor offset responses persist for multiple seconds after the odor exposure (Alvarez-Salvado et al., 2018; Sayin et al., 2019). In our experiments with semi head-compressed flies, we found that, similar to previous reports, flies increase their turning rate upon brief stimulation with food odor apple cider vinegar (Figure 5B). During these experiments, we were able to capture odor evoked neural responses from all of the mushroom body γ-lobe compartments reliably (Figure 5C).

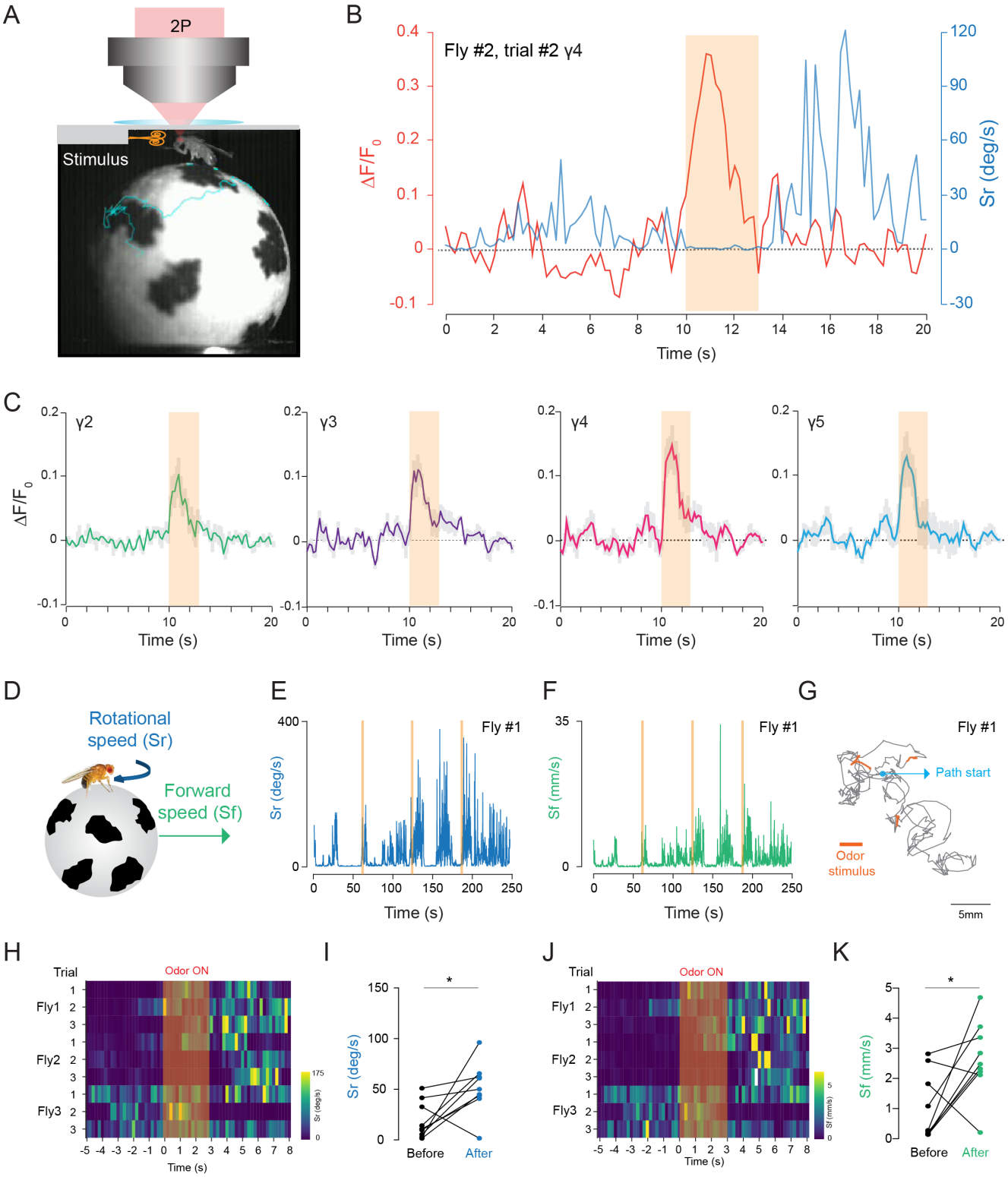

Figure 5. 2P functional imaging of odor-evoked responses in walking flies. (A) Schematic of the custom-made odor delivery and spherical treadmill system. (**B**) Odor evoked response in mushroom body $\gamma 4$ compartment is overlaid with the rotational speed (Sr) measured at the same time. **(C)** Normalized ($\Delta F/F_0$) GCaMP6s signal is shown during the odor stimulation experiments. Odor-evoked responses of Kenyon cells are captured by 2P excitation at 920 nm (n=3 flies, 3 trials per fly, data are presented as mean ± SEM). (**D**) Schematics showing measurements of the rotational and forward speed of flies on the spherical treadmill. (**E-G**) Representative plots for a single fly during the odor stimulation experiments showing rotational speed (Sr) (**E**), forward speed (Sf) (**F**) as a function of time, and the total calculated 2D fictive path (**G**). (**H-K**) Summary heatmap plots and statistical comparison for rotational (**H-I**) and forward speed (**J-K**) 5 seconds before and after the odor stimulation (n=3 flies, 3 trials per fly, paired-two tail t-test, p=0.0225). Average laser power at 920 nm is <10mW**.**

297 We further analyzed the odor evoked changes in fly walking behavior and showed that after the brief
298 exposure to food odor stimulus, flies increased their forward walking speed and turning rate (Figure
299 5E-G). These responses lasted for multiple seconds (Figure 5H-K). Moreover, statistical analysis
300 showed that there is a significant difference between the average forward and rotational speed values
301 before and after the food odor exposure (Figure 5I&K). Our results are in agreement with previous
302 studies that quantified odor induced changes in walking behavior in head fixed flies (Sayin et al., 2019).
303 Altogether, these results indicate that head-compressed flies in our spherical treadmill setup can walk
304 and exhibit behavioral and neural responses to odor stimulation.
305

306 **2P through-cuticle imaging captures chronic odor evoked responses**

307 Studying how neural circuits change activity during learning or in alternating behavioral states requires
308 non-invasive chronic imaging methods that permit recording neural activity over long time scales.
309 Leveraging the non-invasive nature of our preparation, we pushed the limits of functional imaging of
310 the fly brain in response to food odor stimulation to longer time scales (12 hours). Using our custom
311 odor delivery system, we stimulated the fly antenna with food odor (apple cider vinegar) every four
312 hours while imaging through the head cuticle using 2P excitation (920 nm) (Figure 6A). We calculated
313 the normalized peak fluorescent signal per fly in each γ-lobe compartment and time point as a metric
314 representing the food odor response strength during chronic imaging (Figure 6B-E). Our analysis
315 showed that the odor-evoked neural responses did not change with food and water deprivation in any
316 of the γ-lobe compartments imaged (Figure 6F). During these long-term imaging experiments, we
317 captured the fly's behavior in parallel with the odor stimulation to assure that the fly stayed alive during
318 long-term imaging. These results suggest that the non-invasive imaging method developed here allows
319 recording of neural activity within an individual fly over long-time scales (12hours), which was previously
320 not possible with commonly used open-cuticle imaging methods.

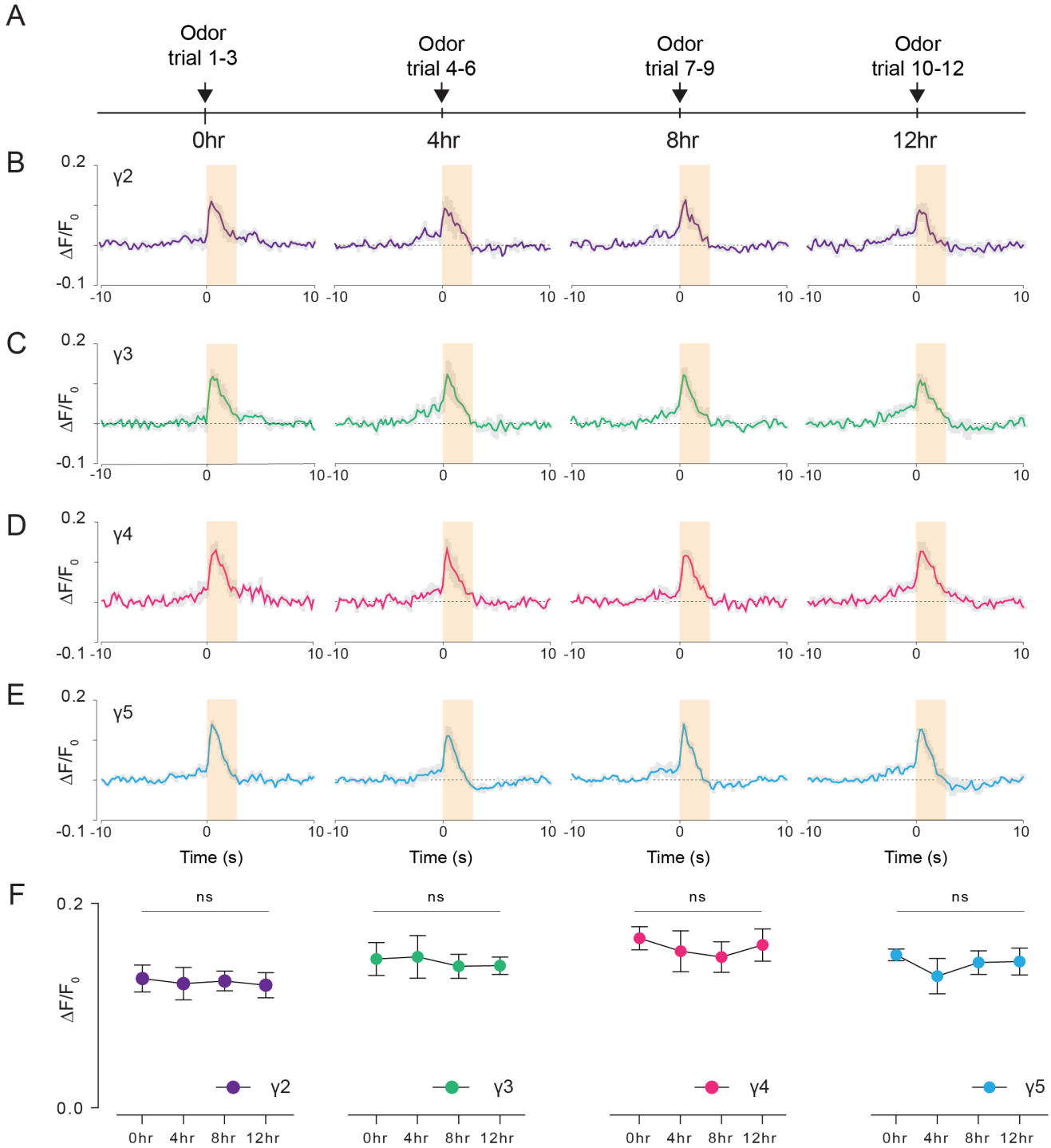

Figure 6. Long-term 2P imaging of odor-evoked responses of the mushroom body γ-lobes **(A)** Stimulus timeline for long-term odor imaging. GCaMP6s fluorescence signal is captured from Kenyon cells axons innervating mushroom body γ-lobes using the semi-compressed preparation. (**B-E)** Quantification of the normalized signal ($\Delta F/F_0$) over time in each γ-lobe compartment. Light orange bar indicates when the odor stimulus is present. Each colored line indicates the average response of a fly over multiple trials in a given hour. The average response of 3 flies is shown. Each compartment's response is labelled with a different color. **(F)** Quantification of the peak amplitude across different time points and lobes ($\Delta F_{max}/F_0$) (Two-way repeated measures ANOVA. Data are presented as mean ± SEM, ns= not significant, n=3 flies, 3 trials per time point). Average laser power at 920 nm is <10mW.

330 **Discussion**

331 Imaging through the fly cuticle was considered to be difficult at the wavelengths typically used for 2P
332 (~ 920 nm) and 3P (~ 1300 nm) imaging because of concerns about cuticle absorption (Lin et al., 2015;
333 Tao et al., 2017). By quantitatively measuring the optical properties of the fly cuticle at wavelengths
334 that correspond to 2P and 3P fluorescence imaging, we discovered that fly cuticle transmit long
335 wavelength light with surprisingly high efficiency (Figure 1), and it is not the absorption by the cuticle
336 but rather the opacity of the air sacs and tissues located between the head cuticle and the brain that
337 limit the penetration depth of multiphoton imaging (Video 2). This new understanding of the challenges
338 for through-cuticle imaging clearly indicated that long excitation wavelength (e.g., ~ 1700 nm) is not
339 necessary for non-invasive imaging through the fly cuticle. By compressing the fly head using a glass
340 coverslip, we reduced the volume of the heterogenous tissues between the cuticle and the brain, which
341 increases the transmission of laser light and therefore allows high resolution, non-invasive imaging of
342 the fly brain through the intact cuticle (Figure 2). Careful assessments showed that such a head
343 compression does not cause measurable differences in fly behaviors (Figure 5). Our fly preparation
344 method enabled non-invasive 2P and 3P imaging of common fluorophores (e.g., GFP and GCaMPs)
345 through the intact cuticle at 920 nm and 1320 nm, respectively (Figure 2-6). While we did not see
346 noticeable differences in the recorded activity traces when performing simultaneous 2P and 3P
347 functional imaging of the mushroom body, 3P imaging has higher contrast than 2P imaging in the
348 deeper regions of the fly brain such as the central complex.

349 Investigating how physiological states, sleep, and learning change the function of neural circuits
350 requires tracking the activity of molecularly defined sets of neurons over long time scales. These
351 experiments require non-invasive, long term imaging methods to record neural activity *in vivo*. The non-
352 invasive through-cuticle imaging method developed here significantly extends the time frame of current
353 *in vivo* imaging preparations used for anatomical and functional studies in fly neuroscience. Non-
354 invasive imaging of the fly brain will allow us to capture the activity of neural populations during
355 changing behavioral states; facilitate decoding of neural plasticity during memory formation; and permit
356 observation of changes in brain structures during development and aging. Our first demonstration of
357 long-term functional imaging of the fly brain captures food odor responses from mushroom body γ-
358 lobes for up to 12 hours continuously. Our results suggest that odor evoked Ca^{2+} responses did not
359 change during the repeated odor stimulation. Even longer imaging time is possible by feeding flies

360 under the microscope. We performed 2P imaging for demonstrating the possibility of long term
361 recording of neural activity because conventional 2P microscopy has adequate penetration depth for
362 imaging the behavioral responses within the mushroom body, and 2P microscopy is widely used by the
363 neuroscience community. On the other hand, our deep imaging data (Figure 3A) showed that the
364 combination of our fly preparation and 3P imaging may provide the exciting possibility of long-term
365 imaging through the entire depth of the fly brain through the intact cuticle.

366 Our focus here was to develop non-invasive in vivo structural and functional imaging methods
367 that can extend imaging quality and length for the fly brain. We anticipate that there will be a wide
368 variety of uses for this technology in *Drosophila* neuroscience research.

369

370 **Acknowledgements**

371 We thank Joe Fetcho, Andy Bass, David Owald, and members of the Yapici Lab for comments on the
372 manuscript. We acknowledge Bloomington Drosophila Stock Centre (NIH P40OD018537) and the
373 Developmental Studies Hybridoma Bank (NICHD of the NIH, University of Iowa) for reagents. We thank
374 Li Yan McCurdy (Yale University) and Matt Einhorn (Cornell University) for help with the design and
375 construction of the custom built olfactometer, and Nancy M. Bonini (University of Pennsylvania) for her
376 advice on the HSP70 antibody. Research in N.Y.'s laboratory is supported by a Cornell University
377 Nancy and Peter Meinig Family Investigator Program, a Pew Biomedical Scholar Award, the Alfred P.
378 Sloan Foundation Award, AFAR Research Grant for Junior Faculty, NSF NeuroNex Program Grant
379 (DBI-1707312), and NIH R35 ESI-MIRA Grant (R35GM133698-01).

380

381 **Author contributions**

382 The authors have made the following declarations about their contributions: Conceived and supervised
383 the study: C.X., and N.Y. Designed the experiments: M.J.A, M.W., J.S., A.M., C.X., and N.Y. Performed
384 the experiments: J.S. and A.M. (Figure 1,5,6), M.J.A., and M.W. (Figure 2-4), H.K. (Figure 4-figure
385 supplement 1), N.B. (Figure 1). Analyzed the data and prepared figures: M.J.A., M.W, J.S., A.M., H.K.,
386 and N.Y. Wrote the paper: N.Y. with input from C.X., M.J.A., M.W., J.S., A.M., and H.K.

387 **Materials and Methods**

388 **Fly stocks**

389 Flies were maintained on conventional cornmeal-agar-molasses medium at 23-25°C and 60-70%
390 relative humidity, under a 12hr light: 12hr dark cycle (lights on at 9 A.M.). Fly strains and sources: *Mef2-*
391 *GAL4* (Bloomington # 50742); *GMR15B07-GAL4* (Bloomington # 48678), *10XUAS-IVS-mCD8::GFP*
392 (Bloomington # 32186); *20XUAS-IVS-GCaMP6s* (Bloomington # 42746); *GMR57C10-GAL4*
393 (Bloomington # 39171).

394

395 **Detailed genotypes of all fly strains used in the paper are as follows**

396 ***Figure 1***

397 *Males, w^{1118}/Y; 20XUAS-IVS-GCaMP6s; Mef2-GAL4.*

398 ***Figure 2***

399 *Males, w^{1118}/Y; 10XUAS-IVS-mCD8::GFP; Mef2-GAL4.*

400 ***Figure 2- figure supplement 1***

401 *Males, w^{1118}/Y; 10XUAS-IVS-mCD8::GFP; Mef2-GAL4.*

402 ***Figure 3***

403 *Panel A-D: Males, w^{1118}/Y; 10XUAS-IVS-mCD8::GFP; GMR57C10.*

404 *Panel E-G : Males, w^{1118}/Y; 10XUAS-IVS-mCD8::GFP; GMR15B07-GAL4.*

405 ***Figure 3- figure supplement 1***

406 *Males, w^{1118}/Y; 10XUAS-IVS-mCD8::GFP; GMR15B07-GAL4.*

407 ***Figure 4-6***

408 *Males, w^{1118}/Y; 20XUAS-IVS-GCaMP6s; Mef2-GAL4.*

409 ***Figure 4- figure supplement 1***

410 *Males, w^{1118}/Y; 20XUAS-IVS-GCaMP6s; Mef2-GAL4.*

411 **Optical transmission measurements of the fly head cuticle**

412 Drosophila cuticle was dissected from the dorsal head capsule of flies that are age and gender
413 controlled (male, 5 days old). The dissected cuticle was sandwiched between two #1 coverslips (VWR
414 #1 16004-094) with ~10 μL of UV curable resin (Bondic UV glue #SK8024) to avoid dehydration of the
415 sample (Figure 1A). Measurements from each dissected cuticle was done within a day. The first several
416 measurements were repeated at the end of all measurements to ensure that dehydration or protein
417 degradation, which may affect the optical properties of the tissue, did not happen as the experiment
418 progressed. The total transmission and ballistic transmission of cuticle samples were measured using
419 a custom-built device (Figure 1B). For ballistic transmission experiments, light from a single-mode fiber
420 was magnified and focused on the cuticle with a ~25μm spot size. We assume that collimated light
421 passes through the sample since the Rayleigh range for a 25μm ($1/e^2$) focus spot is approximately
422 1mm - 2mm for wavelengths between 852 nm and 1624 nm, which is much larger than the thickness
423 of the entire coverslip sandwich-prep (<400μm). The transmitted light from the cuticle was then coupled
424 to another single-mode fiber with identical focusing optics and detected with a power meter (S146C,
425 Thorlabs). Such a confocal setup ensures that only the ballistic transmission is measured. The incident
426 power is ~10mW on the cuticle for each measurement. An InGaAs camera (WiDy SWIR 640U-S, NiT)
427 and a CMOS camera (DCC1645C, Thorlabs) were used to image the sample and incident beam to
428 ensure that the incident light spot is always on the cuticle and to avoid the dark pigments (usually at
429 the edge of the cuticle), ocelli, and possible cracks introduced during dissection. The ballistic
430 transmission of the cuticle was then calculated as the power ratio between the ballistic transmissions
431 through the cuticle (PT^{SMF}) and the surrounding areas without the cuticle (PT_0^{SMF}), i.e., a reference
432 transmission through areas containing only the UV curable resin, using the equation below:

433 $$T_{ballistic} = \frac{PT^{SMF}}{PT_0^{SMF}}$$

434 For measuring the total transmission, light from a single-mode fiber was magnified and focused on the
435 cuticle with a ~50μm spot size. We again assume that collimated light passes through the sample since
436 the Rayleigh range for a 50μm ($1/e^2$) spot size is 5mm - 10mm for wavelengths between 532 nm and
437 1624 nm. An integrating sphere power meter (S146C, Thorlabs) is placed immediately after the sample
438 to measure the total transmission. The incident power on the sample is ~10mW. The same cameras
439 were used to visualize the light spot and the cuticle when the integrating sphere is removed. The total

440 transmission of the cuticle was then calculated as the optical power ratio between the transmissions
441 through the cuticle (PT^{IS}) and the reference transmission through areas containing only the UV curable
442 resin (PT_0^{IS}), both measured by the integrating sphere (IS).

443 $$T_{total} = \frac{PT^{IS}}{PT_0^{IS}}$$

444 Data in Figure 1D&G are acquired by manually translating the sample orthogonal to the light path. For
445 Figures 1E and 1H, the samples were translated with a motorized stage to acquire a spatially-resolved
446 transmission map. We collected data from several locations for each wavelength (ballistic transmission,
447 n=56 measurements across 5 cuticle samples; total transmission, n=20 measurements across 4
448 samples). We then calculated the mean and the standard error across all measurements for ballistic or
449 total transmission for the plots shown in Figure 1D&G respectively.

450

451 **Through-cuticle *in vivo* imaging preparation**

452 All animals used for imaging experiments were male flies with indicated genotypes kept at 25°C
453 incubators and maintained on conventional cornmeal-agar-molasses medium. Flies used for chronic
454 functional experiments were 2-7 days old, and flies used for short term functional experiments were 1-
455 4 days old. To perform through-cuticle brain imaging, flies were first head-fixed in a 40 mm weigh dish
456 (VWR#76299-236) with a hole made with forceps. A drop of UV curable resin (Liquid plastic welder,
457 Bondic®) was applied to the head and thorax, which was then cured with blue light (~470 nm) and
458 fused to a cover glass. The fly antennae are ensured to be full exposed after curing. Fly proboscises
459 were immobilized with blue light curable resin to minimize head motion caused by muscle contractions.
460 Video 1 explains the details of the imaging preparation. Only flies in Figure 2-figure supplement 1 went
461 through surgery to remove the air sacs using a sharp needle.

462

463 **Multiphoton Excitation source**

464 Whole brain 2P/3P imaging: The 3P excitation source is a wavelength-tunable optical parametric
465 amplifier (NOPA, Spectra-Physics) pumped by a femtosecond laser (Spirit, Spectra-Physics) with a
466 MOPA (Master Oscillator Power Amplifier) architecture. The center wavelength is set at 1320 nm. An
467 SF11 prism pair (PS853, Thorlabs) is used for dispersion compensation in the system. The laser

468 repetition rate is maintained at 333kHz. The 2P excitation source is a Ti:Sapphire laser centered at 920
469 nm (Chameleon, Coherent). The laser repetition rate is at 80MHz.
470 3P imaging: The excitation source is a wavelength-tunable optical parametric amplifier (OPA, Opera-
471 F, Coherent) pumped by a femtosecond laser (Monaco, Coherent) with a MOPA (Master Oscillator
472 Power Amplifier) architecture. The center wavelength is set at 1320 nm. An SF10 prism pair (10SF10,
473 Newport) is used for dispersion compensation in the system.
474 Simultaneous 2P/3P imaging and 2P imaging: The 3P excitation source is a wavelength-tunable optical
475 parametric amplifier (NOPA, Spectra-Physics) pumped by a femtosecond laser (Spirit, Spectra-
476 Physics) with a MOPA (Master Oscillator Power Amplifier) architecture. The center wavelength is set
477 at 1320 nm. An SF11 prism pair (PS853, Thorlabs) is used for dispersion compensation in the system.
478 The laser repetition rate is maintained at 400kHz. The 2P excitation source is a Ti:Sapphire laser
479 centered at 920 nm (Tsunami, Spectra-Physics). The laser repetition rate is at 80MHz.
480
481 **Multiphoton microscopes**
482 Whole brain 2P/3P imaging: It is taken with a commercial multiphoton microscope with both 2P and 3P
483 light path (Bergamo II, Thorlabs). A high numerical aperture (NA) water immersion microscope
484 objective (Olympus XLPLN25XWMP2, 25X, NA 1.05) is used. For GFP and THG imaging, fluorescence
485 and THG signals are separated and directed to the detector by a 488 nm dichronic mirror (Di02-R488,
486 Semrock) and 562nm dichronic mirror (FF562-Di03). Then the GFP and THG signals are further filtered
487 by a 525/50 nm band-pass filter (FF03-525/50, Semrock) and 447/60 nm (FF02-447/60, Semrock)
488 band-pass filter, respectively. The signals are finally detected by GaAsP PMTs (PMT2101, Thorlabs).
489 3P imaging: A scan lens with 36mm focal length (LSM03-BB, Thorlabs) and a tube lens with 200mm
490 focal length are used to conjugate the galvo mirrors to the back aperture of the objective. The same
491 high numerical aperture (NA) water immersion microscope objective (Olympus XLPLN25XWMP2, 25X,
492 NA 1.05) is used. Two detection channels are used to collect the fluorescence signal and the third
493 harmonic generation (THG) signal by photomultiplier tubes (PMT) with GaAsP photocathode (H7422-
494 40, Hamamatsu). For 3-photon imaging of GFP and GCaMP6s at 1320 nm, fluorescence signal and
495 THG signal were filtered by a 520/60 nm band-pass filter (FF01-520/60-25, Semrock) and a 435/40 nm
496 band-pass filter (FF02-435/40-25, Semrock), respectively. For signal sampling, the PMT current is
497 converted to voltage and low-pass filtered (200 kHz) by a transimpedance amplifier (C7319,

498 Hamamatsu). Analog-to-digital conversion is performed by a data acquisition card (NI PCI-6110,
499 National Instruments). ScanImage 5.4-Vidrio Technologies (Pologruto et al., 2003) running on MATLAB
500 (MathWorks) is used to acquire images and control a movable objective microscope (MOM, Sutter
501 Instrument Company).
502 Simultaneous 2P/3P imaging and 2P imaging: A scan lens (SL50-3P, Thorlabs) and tube lens (TL200-
503 3P, Thorlabs) are used to conjugate the galvo mirrors to the back aperture of the objective. The same
504 objective (Olympus XLPLN25XWMP2, 25X, NA 1.05) is used. Fluorescence signal are detected by
505 photomultiplier tubes (PMT) with GaAsP photocathode (H7422-40, Hamamatsu). For GFP and
506 GCaMP6s imaging, fluorescence signal passes through a 466 nm dichronic mirror (Di02R-466) and
507 filtered by a 520/60 nm band-pass filter (FF01-520/60-25, Semrock). For signal sampling, the PMT
508 current is converted to voltage by a 10-MHz transimpedance amplifier (C9999, Hamamatsu). An
509 additional 1.9-MHz low-pass filter (Minicircuts, BLP-1.9+) was used before digital sampling. Analog-to-
510 digital conversion is performed by a data acquisition card (NI PCI- 6115, National Instruments).
511 ScanImage 3.8 -Vidrio Technologies (Pologruto et al., 2003) running on MATLAB (MathWorks) was
512 used to acquire images.
513
514 **Simultaneous 2P and 3P imaging**
515 Simultaneous imaging with 2P excitation and 3P excitation is achieved by temporal multiplexing of the
516 920 nm Ti:Sapphire laser and 1,320 nm Spirit-NOPA laser. The setup is similar to the one described
517 in a previous study (Ouzounov et al., 2017). Briefly, two lasers were combined with a 980 nm long pass
518 dichronic mirror (BLP01-980R-25, Semrock) and passed through the same microscope. They were
519 spatially overlapped at the same focal position after the objective with a remote focusing module in the
520 2P light path. The 920 nm laser was intensity modulated with an electro-optic modulator (EOM), which
521 was controlled by a TTL waveform generated from a signal generator (33210A, Keysight) that is
522 triggered by the Spirit-NOPA laser. The EOM has high transmission for ~1 μs between two adjacent
523 Spirit-NOPA laser pulses that are 2.5 μs apart. By recording the waveform from the signal generator
524 and the PMT signal simultaneously, the 2P and 3P excited fluorescence signals can be temporally
525 demultiplexed with postprocessing using a custom MATLAB script.
526
527

528 **Preparation of flies used in imaging experiments**

529 Simultaneous 2P/3P functional imaging: Flies were food deprived for 16-24 hours in vials with a wet
530 Kim wipe. Each odor stimulation trial consisted of 50 seconds of clean mineral oil, 3 seconds of
531 undiluted apple cider vinegar stimulus, and another 50 seconds of mineral oil. Between trials, scanning
532 was stopped for 20 seconds to minimize the risk of imaging-induced tissue stress. Five trials were
533 performed sequentially. The images were captured at 80*160-pixel resolution and 13.6 Hz frame rate.

534 2P functional imaging in behaving flies: Flies were head fixed using a custom 3D-printed apparatus
535 which also holds the tube for odor delivery. In this setup, flies are allowed to walk on a spherical
536 treadmill and turn towards the odor stimuli. The odor stimulus is located on the right side of the fly.
537 Each odor stimulation trial consisted of 60 seconds of clean mineral oil, 3 seconds of undiluted apple
538 cider vinegar stimulus, and another 60 seconds of mineral oil. Every change of odor triggers the
539 acquisition software to save in a new file. The images were captured at 256*128-pixel resolution and
540 16.98 Hz frame rate. Three trials were performed sequentially.

541 2P chronic functional imaging: Flies used in long term functional imaging experiments were kept on
542 regular fly food before the first trial to assure that they were satiated. Each odor stimulation trial
543 consisted of 60 seconds of clean mineral oil, 3 seconds of undiluted apple cider vinegar stimulus, and
544 another 60 seconds of mineral oil. Every change of odor triggers the acquisition software to save in a
545 new file. The images were captured at 256*128-pixel resolution and 16.98 Hz frame rate. Three trials
546 were performed sequentially and the three-trial block was repeated every four hours. Between trial
547 blocks, scanning was stopped, and air passing through the stimulation tube was redirected to the
548 exhaust valve to prevent desiccation. To further prevent desiccation, flies were placed on a water-
549 absorbing polymer bead.

550

551 **Stimulus Delivery**

552 Odor delivery during 2P/3P simultaneous functional imaging: Food odor, apple cider vinegar, was
553 delivered using a custom built olfactometer as described previously (Raccuglia et al., 2016). Clean
554 room air was pumped (Active Aqua Air Pump, 4 Outlets, 6W, 15 L/min) into the olfactometer, and the
555 flow rate was regulated by a mass flow controller (Aalborg GFC17). Two Arduino controlled 3-way
556 solenoid valves (3-Way Ported Style with Circuit Board Mounts, LFAA0503110H) controlled air flow.
557 One valve delivered the odorized airstream either to an exhaust outlet or to the main air channel, while

558 another valve directed air flow either to the stimulus or control channel. The stimulus channel contained
559 a 50 ml glass vial containing undiluted apple cider vinegar (volume=10 ml) (Wegmans), while the
560 control channel contained a 50 ml glass vial containing mineral oil (volume=10 ml). Flies were placed
561 approximately 1 cm from a clear PVC output tube (OD = 1.3 mm, ID = 0.84 mm), which passed a ~1<
562 L/min air stream to the antennae. The odor stimulus latency was calculated before the experiments
563 using a photo ionization detector (PID) (Aurora Scientific). We sampled odor delivery using the PID
564 every 20 ms and found average latency to peak odor amplitude was < 100ms across 34 measurements.
565 Flies were stimulated with air (50s), before and after the odor stimulus (odor + air, 3s). Same stimulus
566 scheme was repeated 3 times.
567 Odor delivery during spherical treadmill and chronic imaging**:** An air supported spherical treadmill setup
568 was used to record fly walking behavior during multiphoton imaging. Male flies at 5-6 days post eclosion
569 were anesthetized on ice for about 2 minutes and mounted to a coverslip with semi-compression as
570 described in Video 1. The cover slip was glued to a custom 3D printed holder with an internal airway in
571 order to deliver airflow along the underside of the coverslip directly onto the antenna without interfering
572 with the air supported ball. The air duct was positioned 90 degrees to the right of the fly about 1cm
573 away. Clean room air was pumped (Hygger B07Y8CHXTL) into a mass flow meter set at 1L/min
574 (Aalborg GFC17). The regulated airflow was directed through an Arduino controlled three-way solenoid
575 pinch valve (Masterflex UX-98302-42) using 1/16" ID tubing. The valve directed the airflow either
576 through 50ml glass vile containing 10ml of undiluted apple cider vinegar for the stimulus, or through a
577 50ml glass vile containing 10ml of mineral oil for the control. The latency from stimulus signal from the
578 Arduino to odor molecules arriving at the fly's antenna was measured using a photo-ionization detector
579 (Aurora Scientific) prior to the experiments and found to be <200ms to peak stimulus.
580
581 **Fly behavior**
582 The spherical treadmill was manufactured by custom milling with 6061 aluminum alloy. The treadmill
583 has a concave surface at the end for placing the ball, which is supported by airflow. We fabricated foam
584 balls (Last-A-Foam FR-7110, General Plastics, Burlington Way, WA USA) that are 10mm in diameter
585 using a ball-shaped file. We drew random patterns with black ink on the foam balls to provide a high-
586 contrast surface for the ball tracking analysis. Fly behavior was videotaped from the side to capture
587 any movement by a CCD camera (DCC1545M, Thorlabs) equipped with a machine vision camera lens

588 (MVL6X12Z, Thorlabs) and 950 nm long pass filter (FELH0950, Thorlabs). The acquisition frame rate
589 for video recording was set to 8Hz under IR light illumination at 970 nm (M970L4, Thorlabs). The
590 stimulus signal from the Arduino is captured by NI-6009 (National Instrument) using a custom script
591 written in MATLAB 2020b (Mathworks) to synchronize with the behavior video in data analysis.
592

593 **Image processing and data analysis**

594 Resolution measurements: We measured the lateral brightness distribution of small features within the
595 fly brains using either the GFP fluorescence signal (Figure 3F) or the THG signal (Figure 3D&G). Lateral
596 intensity profiles measured along the white lines were fitted by a Gaussian profile for the estimation of
597 the lateral resolution.

598 Measurement of excitation light attenuation in the fly brain: The image stack was taken with 5 μm step
599 size in depth, and the imaging power was increased with imaging depth to keep the signal level
600 approximately constant. The signal (S) of each frame was calculated as the average of the brightest
601 0.25%-pixel values and then normalized by the imaging power (P) on the fly surface. The normalization
602 is S/P^2 and S/P^3 for the 2P and 3P stacks, respectively. The effective attenuation length (EAL) is then
603 derived by least-squares linear regression of the normalized fluorescence or THG signal at different
604 imaging depth (Figure 3B&C).

605 Image processing for structural imaging. TIFF stacks containing fluorescence and THG data were
606 processed using Fiji, an open-source platform for biological-image analysis (Schindelin et al., 2012).
607 When necessary, stacks were registered using the TurboReg plugin.

608 Multiplex 2P and 3P functional imaging: TIFF stacks containing fluorescence data were converted to
609 32 bits, and pixel values were left unscaled. Lateral movement of the sample in the image series, if
610 any, was corrected by TurboReg plug-in in ImageJ. Images acquired during the multiplexed 2P-3P
611 imaging sessions were first median filtered with a filter radius of 10 pixels to reduce high amplitude
612 noise. To compute $\Delta F/F_0$ traces, γ-lobe ROIs were first manually selected using a custom Python script.
613 F_0 was computed as the average of 10 frames preceding stimulus onset. The F_0 image was then
614 subtracted from each frame, and the resulting image was divided by F_0. The resulting trace was then
615 low-pass filtered by a moving mean filter with a window size of 8 frames. Data were analyzed using

616 Python and plotted in Microsoft Excel. Peak $\Delta F/F_0$ was determined by the peak value within 20 frames
617 after the odor delivery.
618 2P functional imaging in behaving flies and chronic functional imaging: Lateral movement of the sample
619 in the image series, if any, was corrected by TurboReg plug-in in ImageJ. A custom script written in
620 MATLAB 2016b is used for all subsequent processing. Every 4 frames are averaged to achieve an
621 effective frame rate of 4.25 Hz. Regions of interest (ROIs) were generated by manual segmentation of
622 the mushroom bodies. The baselines of the activity traces (F0) for each ROIs are determined using a
623 rolling average of 4s over the trace after excluding data points during odor stimulation. The activity
624 traces (F) were normalized according to the formula $(F - F_0)/F_0$. The trace is finally resampled to 5Hz
625 with spline interpolation to compile with the timing in the motion tracking trace.
626 Fly walking behavior analysis: Fly walking traces were obtained using the FicTrac (Fictive path
627 Tracking) software as published previously (Moore et al., 2014). The ball rotation analysis was
628 performed using the 'sphere_map_fn' function, which allows the use of a previously generated map of
629 the ball to increase tracking accuracy. We post-processed the raw output generated by FicTrac. To
630 calculate forward and rotational speeds, we used the delta rotation vectors for each axis. Then, we
631 down-sampled raw data from 8Hz to 5Hz by averaging the values in the 200ms time-windows. The
632 empty data points generated from down-sampling were linearly interpolated. All FicTrac analysis were
633 done using a custom Python code.
634
635 **Immunohistochemistry for brain tissue damage assessment**
636 To investigate laser-induced stress in the fly brain during 3-photon imaging through the intact head
637 cuticle, 1-2-day old male homozygous MB>GCaMP6s flies were imaged continually at 1320 nm for 10
638 minutes. The laser was focused 70μm below the cuticle with ~20mW or ~25mW average power. Flies
639 were head compressed to reproduce actual experimental conditions. Laser exposed brains were
640 dissected approximately 2 hours after mounting. To test HSP70 antibody efficacy on fly brains, a
641 positive control group of flies was first exposed to 30°C for 10 minutes in an incubator to induce HSP70
642 expression. Negative control group of flies was kept at room temperature. For whole mount staining,
643 brains were dissected in phosphate-buffered saline (PBS) and incubated in 4% paraformaldehyde
644 (PFA) in PBS for 20-30 minutes at room temperature on an orbital shaker. Tissues were washed 3-4

645 times over 1 hour in PBS (calcium- and magnesium-free; Lonza BioWhittaker #17-517Q) containing
646 0.1% Triton X-100 (PBT) at room temperature. Samples were blocked in 5% Normal Goat Serum in
647 PBT (NGS-PBT) for 1 hour and then incubated with primary antibodies diluted in NGS-PBT for 24 hours
648 at 4°C. Primary antibodies used were anti-GFP (Torrey Pines, TP40, rabbit polyclonal, 1:1000), anti-
649 BRP (DSHB, nc82, mouse monoclonal, 1:20), and anti-HSP70 (Sigma, SAB5200204, rat monoclonal,
650 1:200). The next day, samples were washed 5-6 times over 2 hours in PBT at room temperature and
651 incubated with secondary antibodies (Invitrogen) diluted in NGS-PBT for 24 hours at 4°C. On the third
652 day, samples were washed 4-6 times over 2 hours in PBT at room temperature and mounted with
653 VECTASHIELD Mounting Media (Vector Labs, Burlingame, CA, USA) using glass slides between two
654 bridge glass coverslips. The samples were covered by a glass coverslip on top and sealed using clear
655 nail polish. Images were acquired at 1024x1024 pixel resolution at ~1.7 μm intervals using an upright
656 Zeiss LSM 880 laser scanning confocal microscope and Zeiss digital image processing software ZEN.
657 Maximum projection images of Z-stacks were generated in the ZEN image-processing software. The
658 power, pinhole size and gain values were kept the same for all imaged brains during confocal
659 microscopy.

660 **Statistics**

661 Sample sizes used in this study were based on previous literature in the field. Experimenters were not
662 blinded in most conditions as almost all data analysis were automated and done using a standardized
663 computer code. All statistical analysis was performed using Prism 9 Software (GraphPad, version
664 9.0.2). Comparisons with one variable were first analyzed using one-way ANOVA followed by Tukey's
665 multiple comparisons post-hoc test. Comparisons with more than one variable were first analyzed using
666 two-way ANOVA. Comparisons with repeated measures were analyzed using a paired t-test. P values
667 are indicated as follows: ****$p < 0.0001$; ***$p < 0.001$; **$p < 0.01$; and *$p < 0.05$. Plots labeled with
668 different letters in a given panel are significantly different.

669

670 **Data availability**

671 All data supporting the findings of this study is included in the paper and the supplemental files.

672

673 **Competing financial interests**

674 The authors declare no competing financial interests.

675 **References**

676 Alvarez-Salvado, E., Licata, A.M., Connor, E.G., McHugh, M.K., King, B.M., Stavropoulos, N., Victor,
677 J.D., Crimaldi, J.P., and Nagel, K.I. (2018). Elementary sensory-motor transformations underlying
678 olfactory navigation in walking fruit-flies. Elife *7*.

679 Barron, A.B., Gurney, K.N., Meah, L.F., Vasilaki, E., and Marshall, J.A. (2015). Decision-making and
680 action selection in insects: inspiration from vertebrate-based theories. Front Behav Neurosci *9*, 216.

681 Chen, T.W., Wardill, T.J., Sun, Y., Pulver, S.R., Renninger, S.L., Baohan, A., Schreiter, E.R., Kerr,
682 R.A., Orger, M.B., Jayaraman, V.*, et al.* (2013). Ultrasensitive fluorescent proteins for imaging neuronal
683 activity. Nature *499*, 295-300.

684 Cohn, R., Morantte, I., and Ruta, V. (2015). Coordinated and Compartmentalized Neuromodulation
685 Shapes Sensory Processing in Drosophila. Cell *163*, 1742-1755.

686 Crittenden, J.R., Skoulakis, E.M., Han, K.A., Kalderon, D., and Davis, R.L. (1998). Tripartite mushroom
687 body architecture revealed by antigenic markers. Learn Mem *5*, 38-51.

688 Dickson, B.J. (2008). Wired for sex: the neurobiology of Drosophila mating decisions. Science *322*,
689 904-909.

690 Dong, C.Y., Koenig, K., and So, P. (2003). Characterizing point spread functions of two-photon
691 fluorescence microscopy in turbid medium. J Biomed Opt *8*, 450-459.

692 Grover, D., Katsuki, T., and Greenspan, R.J. (2016). Flyception: imaging brain activity in freely walking
693 fruit flies. Nat Methods *13*, 569-572.

694 Hefendehl, J.K., Milford, D., Eicke, D., Wegenast-Braun, B.M., Calhoun, M.E., Grathwohl, S.A., Jucker,
695 M., and Liebig, C. (2012). Repeatable target localization for long-term in vivo imaging of mice with 2-
696 photon microscopy. J Neurosci Methods *205*, 357-363.

697 Horton, N.G., Wang, K., Kobat, D., Clark, C.G., Wise, F.W., Schaffer, C.B., and Xu, C. (2013). In vivo
698 three-photon microscopy of subcortical structures within an intact mouse brain. Nat Photonics *7*.

699 Huang, C., Maxey, J.R., Sinha, S., Savall, J., Gong, Y., and Schnitzer, M.J. (2018). Long-term optical
700 brain imaging in live adult fruit flies. Nat Commun *9*, 872.

701 Hunt, L.T., and Hayden, B.Y. (2017). A distributed, hierarchical and recurrent framework for reward-
702 based choice. Nat Rev Neurosci *18*, 172-182.

703 Ito, K., Suzuki, K., Estes, P., Ramaswami, M., Yamamoto, D., and Strausfeld, N.J. (1998). The
704 organization of extrinsic neurons and their implications in the functional roles of the mushroom bodies
705 in Drosophila melanogaster Meigen. Learn Mem *5*, 52-77.

706 Ji, N., Freeman, J., and Smith, S.L. (2016). Technologies for imaging neural activity in large volumes.
707 Nat Neurosci *19*, 1154-1164.

708 Krashes, M.J., Keene, A.C., Leung, B., Armstrong, J.D., and Waddell, S. (2007). Sequential use of
709 mushroom body neuron subsets during drosophila odor memory processing. Neuron *53*, 103-115.

710 Lerner, T.N., Ye, L., and Deisseroth, K. (2016). Communication in Neural Circuits: Tools, Opportunities,
711 and Challenges. Cell *164*, 1136-1150.

712 Lin, S., Senapati, B., and Tsao, C.H. (2019). Neural basis of hunger-driven behaviour in Drosophila.
713 Open Biol *9*, 180259.

714 Lin, Y.Y., Wu, M.C., Hsiao, P.Y., Chu, L.A., Yang, M.M., Fu, C.C., and Chiang, A.S. (2015). Three-
715 wavelength light control of freely moving Drosophila Melanogaster for less perturbation and efficient
716 social-behavioral studies. Biomed Opt Express *6*, 514-523.

Lindquist, S. (1980). Varying patterns of protein synthesis in Drosophila during heat shock: implications for regulation. Dev Biol *77*, 463-479.

Luo, L., Callaway, E.M., and Svoboda, K. (2018). Genetic Dissection of Neural Circuits: A Decade of Progress. Neuron *98*, 256-281.

Lutcke, H., Margolis, D.J., and Helmchen, F. (2013). Steady or changing? Long-term monitoring of neuronal population activity. Trends Neurosci *36*, 375-384.

McFarland, D.J. (1977). Decision making in animals. Nature *269*, 15-21.

Minocci, D., Carbognin, E., Murmu, M.S., and Martin, J.R. (2013). In vivo functional calcium imaging of induced or spontaneous activity in the fly brain using a GFP-apoaequorin-based bioluminescent approach. Biochim Biophys Acta *1833*, 1632-1640.

Mok, A.T., Wang, T., Xia, F., Wu, C., and Xu, C. (2019). Simultaneous Two- and Three-photon Imaging of Multilayer Neural Activities with Remote Focusing. Paper presented at: Conference on Lasers and Electro-Optics (San Jose, California: Optical Society of America).

Moore, R.J., Taylor, G.J., Paulk, A.C., Pearson, T., van Swinderen, B., and Srinivasan, M.V. (2014). FicTrac: a visual method for tracking spherical motion and generating fictive animal paths. J Neurosci Methods *225*, 106-119.

Nevin, J.A. (1973). The study of behavior : learning, motivation, emotion, and instinct (Glenview, IL; Brighton: Scott, Foresman).

Ouzounov, D.G., Wang, T., Wang, M., Feng, D.D., Horton, N.G., Cruz-Hernandez, J.C., Cheng, Y.T., Reimer, J., Tolias, A.S., Nishimura, N.*, et al.* (2017). In vivo three-photon imaging of activity of GCaMP6-labeled neurons deep in intact mouse brain. Nat Methods *14*, 388-390.

Owald, D., and Waddell, S. (2015). Olfactory learning skews mushroom body output pathways to steer behavioral choice in Drosophila. Curr Opin Neurobiol *35*, 178-184.

Pfeiffer, K., and Homberg, U. (2014). Organization and functional roles of the central complex in the insect brain. Annu Rev Entomol *59*, 165-184.

Podgorski, K., and Ranganathan, G. (2016). Brain heating induced by near-infrared lasers during multiphoton microscopy. J Neurophysiol *116*, 1012-1023.

Pologruto, T.A., Sabatini, B.L., and Svoboda, K. (2003). ScanImage: flexible software for operating laser scanning microscopes. Biomed Eng Online *2*, 13.

Raccuglia, D., McCurdy, L.Y., Demir, M., Gorur-Shandilya, S., Kunst, M., Emonet, T., and Nitabach, M.N. (2016). Presynaptic GABA Receptors Mediate Temporal Contrast Enhancement in Drosophila Olfactory Sensory Neurons and Modulate Odor-Driven Behavioral Kinetics. eNeuro *3*.

Sayin, S., De Backer, J.-F., Siju, K.P., Wosniack, M.E., Lewis, L.P., Frisch, L.-M., Gansen, B., Schlegel, P., Edmondson-Stait, A., Sharifi, N.*, et al.* (2019). A Neural Circuit Arbitrates between Persistence and Withdrawal in Hungry Drosophila. Neuron *104*, 544-558.e546.

Schindelin, J., Arganda-Carreras, I., Frise, E., Kaynig, V., Longair, M., Pietzsch, T., Preibisch, S., Rueden, C., Saalfeld, S., Schmid, B.*, et al.* (2012). Fiji: an open-source platform for biological-image analysis. Nat Methods *9*, 676-682.

Seelig, J.D., Chiappe, M.E., Lott, G.K., Dutta, A., Osborne, J.E., Reiser, M.B., and Jayaraman, V. (2010). Two-photon calcium imaging from head-fixed Drosophila during optomotor walking behavior. Nat Methods *7*, 535-540.

Seelig, J.D., and Jayaraman, V. (2015). Neural dynamics for landmark orientation and angular path integration. Nature *521*, 186-191.

760 Simpson, J.H., and Looger, L.L. (2018). Functional Imaging and Optogenetics in Drosophila. Genetics
761 *208*, 1291-1309.

762 Sinha, S., Liang, L., Ho, E.T., Urbanek, K.E., Luo, L., Baer, T.M., and Schnitzer, M.J. (2013). High-
763 speed laser microsurgery of alert fruit flies for fluorescence imaging of neural activity. Proc Natl Acad
764 Sci U S A *110*, 18374-18379.

765 Strausfeld, N.J., Hansen, L., Li, Y., Gomez, R.S., and Ito, K. (1998). Evolution, discovery, and
766 interpretations of arthropod mushroom bodies. Learn Mem *5*, 11-37.

767 Svoboda, K., and Yasuda, R. (2006). Principles of two-photon excitation microscopy and its
768 applications to neuroscience. Neuron *50*, 823-839.

769 Tao, X., Lin, H.H., Lam, T., Rodriguez, R., Wang, J.W., and Kubby, J. (2017). Transcutical imaging with
770 cellular and subcellular resolution. Biomed Opt Express *8*, 1277-1289.

771 Tinbergen, N. (1969). The study of instinct (Oxford: Oxford University Press).

772 Trachtenberg, J.T., Chen, B.E., Knott, G.W., Feng, G., Sanes, J.R., Welker, E., and Svoboda, K.
773 (2002). Long-term in vivo imaging of experience-dependent synaptic plasticity in adult cortex. Nature
774 *420*, 788-794.

775 Wang, J.W., Wong, A.M., Flores, J., Vosshall, L.B., and Axel, R. (2003). Two-photon calcium imaging
776 reveals an odor-evoked map of activity in the fly brain. Cell *112*, 271-282.

777 Wang, M., Wu, C., Sinefeld, D., Li, B., Xia, F., and Xu, C. (2018a). Comparing the effective attenuation
778 lengths for long wavelength in vivo imaging of the mouse brain. Biomed Opt Express *9*, 3534-3543.

779 Wang, T., Ouzounov, D.G., Wu, C., Horton, N.G., Zhang, B., Wu, C.H., Zhang, Y., Schnitzer, M.J., and
780 Xu, C. (2018b). Three-photon imaging of mouse brain structure and function through the intact skull.
781 Nat Methods *15*, 789-792.

782 Wang, T., Wu, C., Ouzounov, D.G., Gu, W., Xia, F., Kim, M., Yang, X., Warden, M.R., and Xu, C.
783 (2020). Quantitative analysis of 1300-nm three-photon calcium imaging in the mouse brain. Elife *9*.

784 Wolff, T., Iyer, N.A., and Rubin, G.M. (2015). Neuroarchitecture and neuroanatomy of the Drosophila
785 central complex: A GAL4-based dissection of protocerebral bridge neurons and circuits. J Comp Neurol
786 *523*, 997-1037.

787 Xie, X., Tabuchi, M., Brown, M.P., Mitchell, S.P., Wu, M.N., and Kolodkin, A.L. (2017). The laminar
788 organization of the Drosophila ellipsoid body is semaphorin-dependent and prevents the formation of
789 ectopic synaptic connections. Elife *6*.

790 Yagi, R., Mabuchi, Y., Mizunami, M., and Tanaka, N.K. (2016). Convergence of multimodal sensory
791 pathways to the mushroom body calyx in Drosophila melanogaster. Sci Rep *6*, 29481.

792 Yapici, N., Zimmer, M., and Domingos, A.I. (2014). Cellular and molecular basis of decision-making.
793 EMBO Rep *15*, 1023-1035.

794 Yildirim, M., Sugihara, H., So, P.T.C., and Sur, M. (2019). Functional imaging of visual cortical layers
795 and subplate in awake mice with optimized three-photon microscopy. Nat Commun *10*, 177.

796 Zheng, Z., Lauritzen, J.S., Perlman, E., Robinson, C.G., Nichols, M., Milkie, D., Torrens, O., Price, J.,
797 Fisher, C.B., Sharifi, N.*, et al.* (2018). A Complete Electron Microscopy Volume of the Brain of Adult
798 Drosophila melanogaster. Cell *174*, 730-743 e722.

Supplementary figures

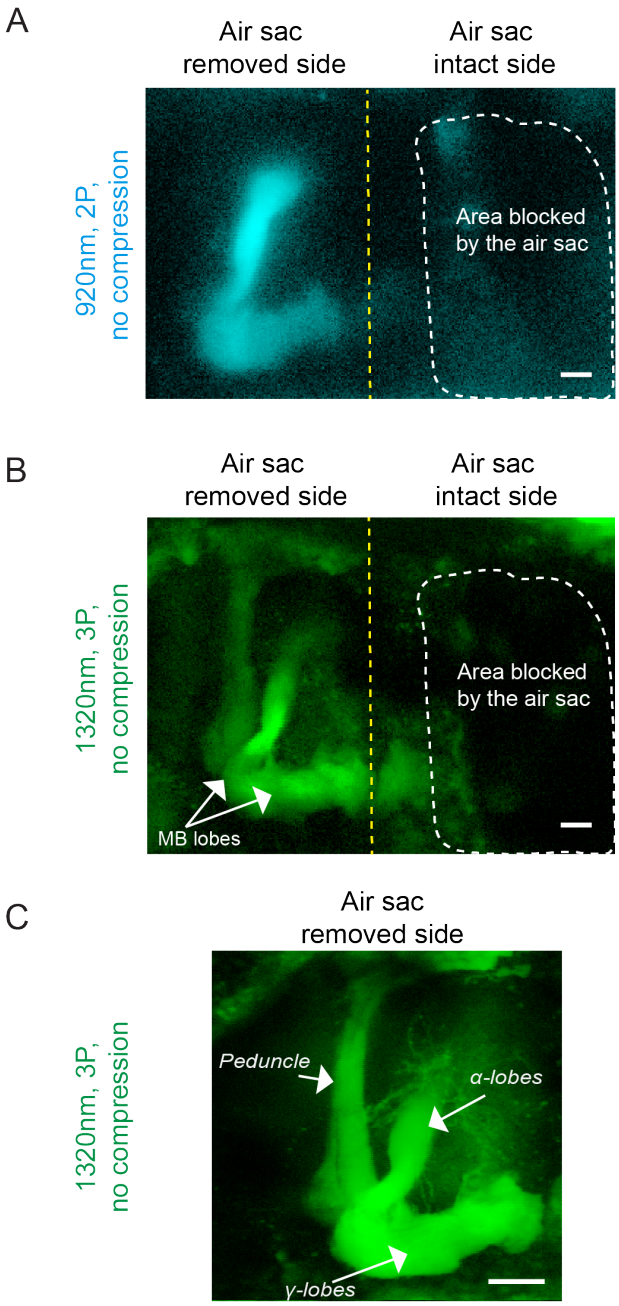

Figure 2– figure supplement 1. Removal of air sacs allows 2P and 3P imaging in a head-uncompressed preparation. Cross section imaging of the mushroom body (MB) Kenyon cells expressing GCaMP6s through the head cuticle at 920 nm (2P) and 1320 nm (3P) excitation after removing air sacs on one side of the head. The fly head is not compressed to the cover slip. The Z projections of **(A)** 2P (cyan) and **(B)** 3P (green) imaging stacks. For each imaging preparation, the same fly brain is imaged with 3P excitation and 2P excitation. Mushroom body structures are visible on the side where air sacs are removed. The dotted lines show the area where the air sacs block imaging. **(C)** Zoomed-in 3P image taken from the side of the brain where the air sacs are removed. Mushroom body lobes and peduncle are clearly visible without the head compression (Scale bars = 20μm).

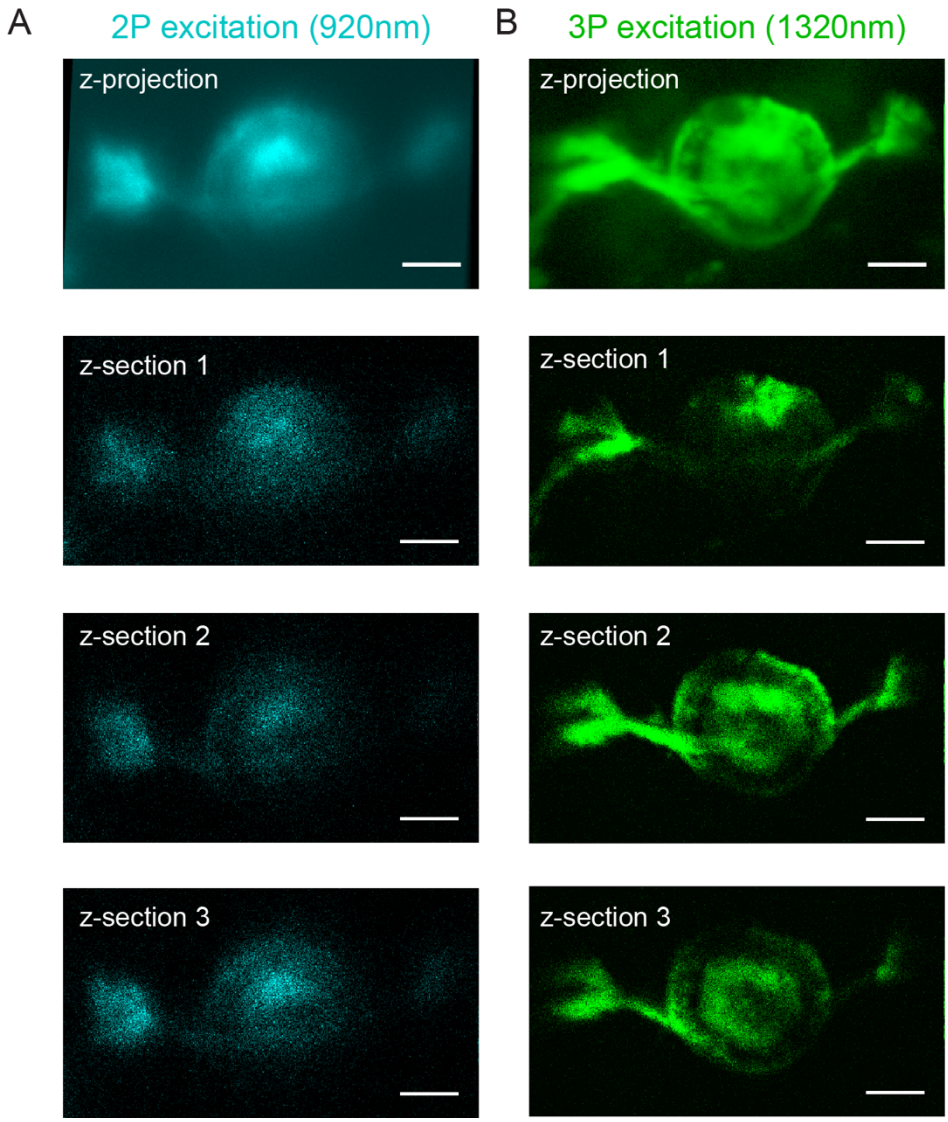

808 **Figure 3– figure supplement 1. Non-invasive imaging of the central complex ring neurons with**
809 **2P and 3P excitation.** Cross section imaging of the Central Complex (CC) ring neurons expressing
810 CD8-GFP through the head cuticle at 920 nm (2P) and 1320 nm (3P) excitation. **(A-B)** The Z projection
811 (top-most) and single optical section images at ~10 μm step of ellipsoid body processes. **(A)** 2P (cyan)
812 and **(B)** 3P (green) images are shown. For each imaging preparation, the same fly head is imaged with
813 both 3P and 2P excitation. Scale bars=25μm.

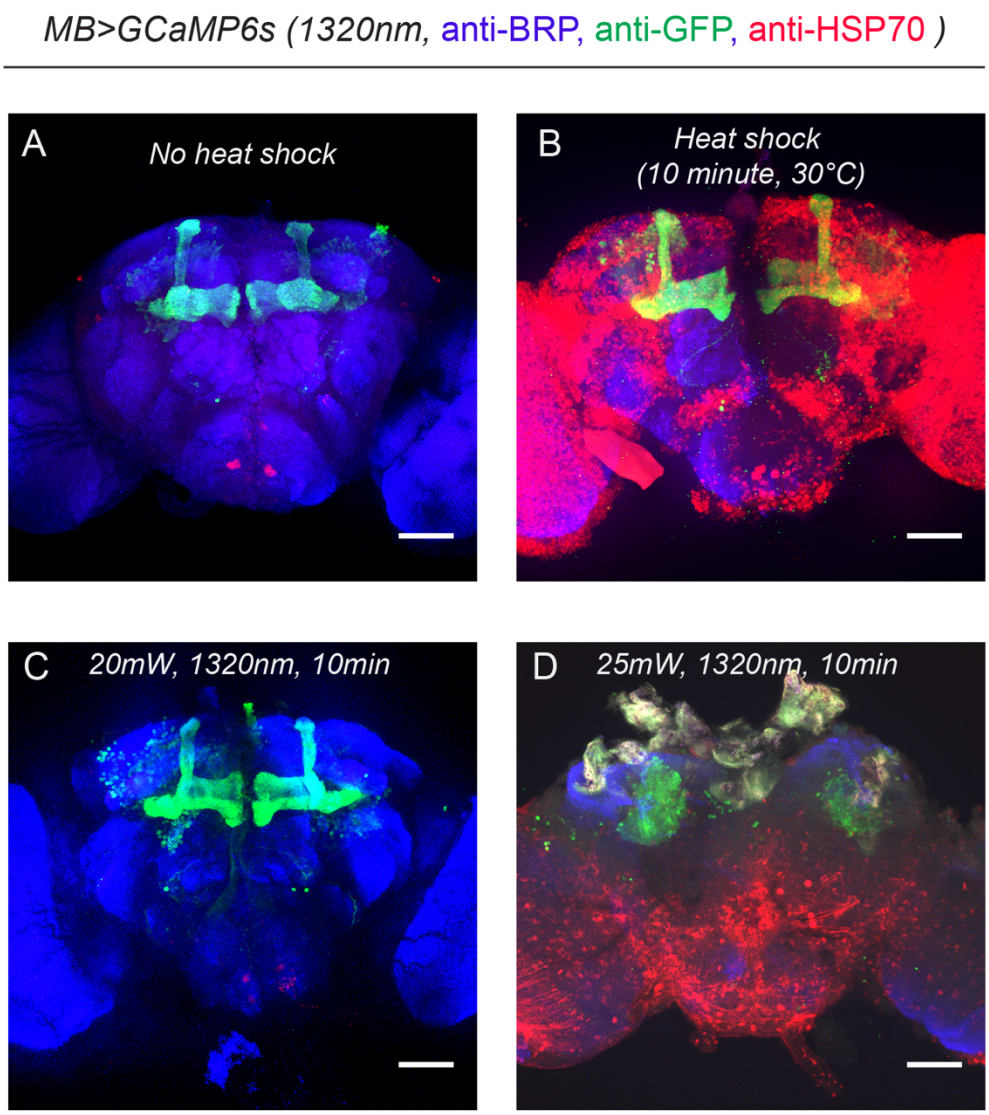

Figure 4– figure supplement 1. HSP70 staining of fly brains after 1320 nm 3P excitation. (A-B) Representative images of fly brains before and after heat shock. **(A)** Without heat shock, there is minimal HSP70 protein expressed in the fly brain. **(B)** When flies are exposed to heat shock (30°C) for 10 minutes, the HSP70 protein expression is significantly elevated across the brain. (**C-D)**, HSP70 protein expression in the fly brain after 3P excitation at 1320 nm for 10 minutes. (**C)** There is no obvious change in HSP70 protein expression when power is <20mW. (**D)** HSP70 protein expression is significantly elevated when power is >25mW. Scale bars = 50µm. The laser power is measured after the microscope objective lens using a power meter (n=2-4 flies per condition).

822 **Video 1: Video demonstrating how to prepare the flies for cuticle-through imaging.**

823

824 **Video 2: Z stack of the mushroom body (MB) Kenyon cells expressing GCaMP6s.** Imaging is
825 done through the head cuticle using 1320 nm (3P) excitation after removing air sacs only on one side
826 of the head (scale bar = 50μm, no head compression).

827

828 **Video 3: Z stack of the ellipsoid body (EB) ring neurons expressing CD8-GFP.**
829 Imaging through the head cuticle at 1320 nm (3P) excitation (scale bar=20μm, semi-compressed prep).

830

831 **Video 4: Neural responses of mushroom body gamma lobes captured through the intact fly**
832 **head cuticle during walking and odor exposure.** Functional imaging is performed in walking flies
833 during a food odor stimulation (apple cider vinegar) with 2P excitation at 920 nm (semi-compressed
834 prep). Video is 5x speed up (Scale bar=30μm).